Steady, inclined flows of granular–fluid mixtures

D. BERZI[1] **AND J.T. JENKINS**[2]

[1]Department of Environmental, Hydraulic, Infrastructures and Surveying Engineering, Politecnico di Milano, Milan 20133, Italy

[2]Department of Theoretical and Applied Mechanics, Cornell University, Ithaca, NY 14853 USA

(Received 3 August 2009)

We extend a recent theory for steady, uniform, gravity-driven flow of a highly concentrated granular–fluid mixture over an erodible bed between frictional sidewalls. We first include angles of inclination greater than the angle of repose of the particles; then, we introduce a boundary condition for flow over a rigid bumpy bed. We compare the predictions of the resulting theory with the volume flow rates, depths, and angles of inclination measured in experiments on dry and variously saturated flows over rigid and erodible boundaries. Finally, we employ the resulting theory, with the assumption that the flow is shallow, to solve, in an approximate way, for the variation of height and average velocities along a steady, non-uniform, inclined flow of a granular–fluid mixture that moves over a rigid bumpy bed. The solutions exhibit features of the flow seen in the experiments - for example, a dry, bulbous snout in advance of the fluid, whose length increases with increasing number of the particles and that disappears with increasing velocity - for which satisfactory explanations were lacking.

1. Introduction

Granular–fluid mixtures driven down a slope by gravity are of great interest in industrial and civil engineering applications. Among the latter, debris flows are probably the best known examples (Takahashi 1991), although a complete, physically-based, mathematical description of such phenomena is still developing (Iverson 1997). Because of the great variety of physical mechanisms involved, the mathematical modelling of highly concentrated mixtures of fluid and granular matter presents a challenge. For example, even in the extremely idealized case of a steady, uniform flow of a mixture of a Newtonian fluid and mono-dispersed particles in a rectangular channel, as in the recent laboratory experiments of Armanini *et al.* (2005) and Larcher *et al.* (2007), inter-particle collisions (e.g. Goldhirsch 2003; Jenkins 2007) and friction (Johnson & Jackson 1987), buoyancy and drag (Iverson 1997), and the influence of boundaries at the bottom (Jenkins & Askari 1991; Jenkins 2001) and the sides (Jop, Forterre & Pouliquen 2005) must be considered. Natural debris flows are also characterized by unsteadiness and non-uniformity (e.g. Davies 1988, 1990), and typically develop through series of surges (Iverson 1997); with complicating factors such as non-hydrostatic pressure (Iverson 1997) and longitudinal variation of particle concentration (Hungr 2000) influencing their behaviour.

Recently, Berzi & Jenkins (2008*a*,*b*) proposed a simple theory based on a linear rheology for the particle interactions, turbulent shearing of the fluid, buoyancy, and drag. They provided a complete analytical description of the steady, uniform flow of a granular–fluid mixture over an erodible bed contained between frictional sidewalls. In order to obtain such analytical solution, they assumed a constant concentration in the particle–fluid layer (that could be considered as the first step in an iterative procedure for the concentration distribution, Berzi & Jenkins 2008*a*) and the similarity of the particle and fluid velocity profiles. The predictions of this analytical description compared favourably with

the measurements in experiments on steady, uniform granular–fluid flows by Armanini *et al.* (2005) and Larcher *et al.* (2007). As experimentally observed, the particle and fluid velocity distributions, the flow depths, and the free surface inclination were completely determined by the particle and fluid volume fluxes. This is a unique feature of the theory; it is a consequence of the particle rheology and the incorporation of the sidewalls forces. As for a dry granular flow between frictional sidewalls (Jop *et al.* 2005), they characterized the erodible bed through a fixed value of the ratio of normal to shear stress (or, equivalently, of the concentration). This gives a relation between particle and fluid depths and angle of inclination of the bed that cannot be obtained if a particle rheology characterized by a constant value of the stress ratio is used (Bagnold 1954; Savage & Hutter 1989; Chen & Ling 1998; Iverson 1997). Actually, Takahashi (1991) improved the Bagnold rheology by using a stress ratio dependent on the concentration. However, he did not provide a criterion to define the position of the erodible bed, and his expression does not reproduce the results of numerical simulations (da Cruz *et al.* 2005; Mitarai & Nakanishi 2007) on dry granular flows. Ancey (2007) places these and other viscoplastic constitutive relations, including that employed here, in the context of regimes exhibited by geophysical flows, including debris flows.

Here, we wish to extend the theory of Berzi & Jenkins (2008*a*,*b*) to steady, uniform, gravity-driven granular–fluid flows at angles of inclination of the free surface greater than the angle of repose of the particles and to incorporate the possibility of flow over a bed that is rigid and bumpy, rather than erodible. As will be shown, this will permit us to reproduce, quantitatively and qualitatively, the relations between flow rates, depths, and inclinations measured in experiments on both dry granular and granular–fluid flows. Furthermore, we will apply our analytical relations between the particle and fluid volume fluxes, the particle and fluid depths and the angle of inclination of the free surface in a

steady, uniform flow to solve, in an approximate, depth-averaged way, the motion of a steady, non-uniform granular–fluid wave over a rigid bumpy bed, experimentally investigated by Davies (1988). In this steady flow, we to neglect any non-hydrostatic pressure effects (Iverson 1997) that are associated with the non-uniformity. We will show that the theory can reproduce the main qualitative features of those flows. In particular, the often observed bulbous shape of those waves naturally results as a consequence of the non-uniformity in the flow depths, without making use of an artificially imposed non-uniformity in the particle concentration (Hungr 2000).

The paper is organized as follows: in § 2, we outline the previous theoretical treatment for steady, uniform flows and extend it to arbitrary angles of inclinations and to flows over a rigid bumpy bed. In the same section, we derive the governing equations of a steady, non-uniform flow over a rigid bumpy bed. In § 3, we compare the predictions of the theory with the results of experiments performed on steady, uniform, dry granular flows (Pouliquen 1999*b*; Taberlet *et al.* 2003; Jop *et al.* 2005) and steady, uniform (Tubino & Lanzoni 1993; Armanini *et al.* 2005) and non-uniform (Davies 1988) granular–fluid flows. Finally, in § 4, we make some concluding remarks.

2. Theoretical framework

In this section, we first briefly summarize the analysis of steady, uniform flows performed in Berzi & Jenkins (2008*a*,*b*) and extend it to flows over an erodible bed at values of the angle of inclination greater than the angle of repose and to flows over a rigid, bumpy bed. Then, we apply the theory to the propagation of a steady granular–fluid wave along an inclined, rigid, bumpy bed experimentally investigated by Davies (1988).

We let ρ denote the fluid mass density, c the particle concentration, g the gravitational acceleration, W the channel width, σ the ratio of particle to fluid density, d the particle

diameter, η the fluid viscosity, U the fluid and u the particle velocity in the flow direction. The Reynolds number $R \equiv \rho d(gd)^{1/2}/\eta$ characterizes the fall velocity of the particles. In what follows, we phrase the momentum balances and constitutive relations in terms of dimensionless variables, with lengths made dimensionless by d, velocities by $(gd)^{1/2}$, and stresses by $\rho\sigma gd$.

2.1. *Steady, uniform, flow*

We take $z = 0$ to be the top of the grains, $z = h$ to be the position of either the erodible or the rigid bed, and H to be the height of the fluid above a bed of inclination ϕ. The inclination of the free surface is θ; it coincides with ϕ in a steady, uniform flow. The degree of saturation, $\xi = H/h$ is greater than unity in the over-saturated case and less than unity in the under-saturated. Sketches of over- and under-saturated flows are depicted in figure 1, together with a generic velocity profile for the particles. In under-saturated flows, when the angle of inclination of the bed is greater than the angle of repose, a layer of thickness ψ at the top of the grains can experience shearing, above a granular plug in the region $\psi \leqslant z \leqslant \zeta$ below it (figure 1b).

We assume that an algebraic relation between the particle shear stress and the granular temperature holds, so that it is possible to apply the rheology proposed by the French group GDR MiDi (2004). Numerical simulations (Silbert *et al.* 2001; Mitarai & Nakanishi 2005) and theory (Jenkins 2006, 2007) indicate that this is true in regions more than ten particle diameters away from the boundaries. Hence, we expect our theory to apply only to thick, dense flows.

This rheology provides the particle stress ratio $\mu \equiv s/p$ and the concentration c as unique functions of the inertial parameter $I \equiv| \dot{\gamma} | /(p/c)^{1/2}$, where s is the particle shear stress, p the particle pressure and $\dot{\gamma}$ is the strain rate. In this case, $| \dot{\gamma} |= -u'$; where here and in what follows, a prime indicates a derivative with respect to z. The inertial parameter

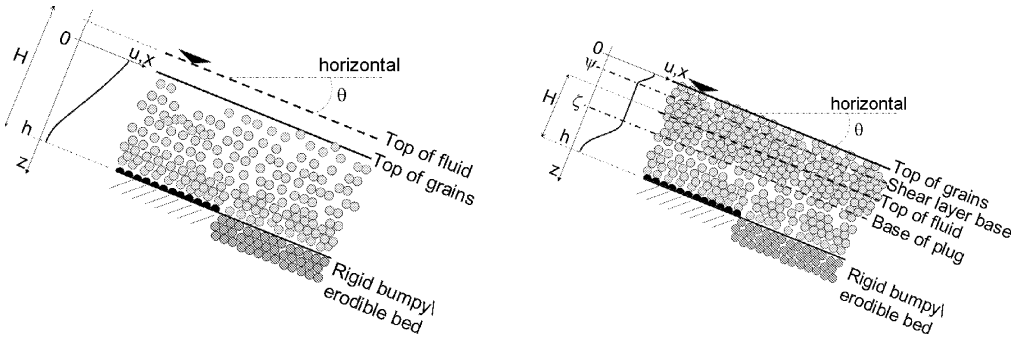

(a) (b)

FIGURE 1. Sketch of steady, (a) over- and (b) under-saturated, uniform flows over erodible or rigid, bumpy beds. Also shown are typical velocity profiles for the particles in the two configurations.

given above represents the ratio between the time scales associated with motion perpendicular and parallel to the flow, respectively, with the former given by the time of free-fall of a particle when the influence of the interstitial fluid is negligible. Cassar *et al.* (2005) have suggested that when the time scale associated with the viscous drag force is much smaller than the time scale associated with a free-fall motion, i.e. when the Stokes number ($S_t = R\sigma\dot{\gamma}/18$) is much smaller than one, the former should be substituted for the latter in the definition of the inertial number. Hence, our analysis is limited to flows characterized by Stokes numbers greater than one. In the experiments performed by Armanini *et al.* (2005) the Stokes number in the flow is everywhere greater than one, except that in a thin layer close to the erodible bed.

We consider highly concentrated flows, in which the aforementioned functions are approximately linear (da Cruz *et al.* 2005):

$$\mu = \breve{\mu} + \chi I, \tag{2.1}$$

and

$$c = \hat{c} - bI, \tag{2.2}$$

where $\check{\mu}$ and $\hat{c}$ are the minimum stress ratio and the maximum concentration, respectively, and χ and b are material coefficients. The quantities $\check{\mu}$ and $\hat{c}$ characterize the erodible bed, at which $I = 0$; $\check{\mu}$ is the tangent of the angle of repose and $\hat{c}$ is the concentration at dense, random packing. We expect (2.1) and (2.2) be valid up to a minimum concentration $\check{c}$ for which the flow can still be considered dense. It has been suggested (Jenkins 2007) that a granular flow is dense when there are correlated motions between the particles; for spheres, this would correspond to concentrations in the range 0.5 to 0.6, approximately. Upon combining (2.1) and (2.2), we determine the stress ratio $\hat{\mu} = \check{\mu} + \chi(\hat{c} - \check{c})/b$ that corresponds to the minimum concentration $\check{c}$. We will show in the following how this largest value of the stress ratio limits the applicability of the present theory.

In order to treat the under-saturated and over-saturated flows in a unified way, Berzi & Jenkins (2008*a*) introduced two auxiliary functions of the degree of saturation ξ:

$$\alpha \equiv 1 + \frac{1}{2}\left(\xi - 1 - \mid \xi - 1 \mid\right) \tag{2.3}$$

and

$$\beta \equiv 1 + \frac{1}{2}\left(\xi - 1 + \mid \xi - 1 \mid\right). \tag{2.4}$$

In an under-saturated flow, $\xi < 1$, $\alpha = \xi$ and $\beta = 1$; while, in an over-saturated flow, $\xi > 1$, $\alpha = 1$, and $\beta = \xi$.

The balances of fluid momentum normal and parallel to the flow in the region $(1-\alpha)h \leqslant z \leqslant h$ in which both phases are present, are

$$P' = \frac{1}{\sigma}\cos\theta \tag{2.5}$$

and

$$S' = (1-c)\frac{1}{\sigma}\sin\theta - \frac{c}{\sigma}C(U-u), \tag{2.6}$$

respectively, where P is the fluid pressure, S is the fluid shear stress, and C is the dimensionless drag:

$$C = \frac{1}{(1-c)^{3.1}}\left(\frac{3}{10} \mid U-u \mid + \frac{18.3}{\mathrm{R}}\right). \tag{2.7}$$

We employ here the expression of the dimensionless drag derived by Dallavalle (1943), with the concentration dependence suggested by Richardson & Zaki (1954). When an upper clear fluid layer is present, the distribution of the fluid shear stress can be obtained from (2.6) with $c = 0$. In (2.6), we ignore the fluid drag at the walls which could play a significant role for flows in narrow channels (less than 10 diameters wide, Richard *et al.* 2009).

The balances of particle momentum normal and parallel to the flow, for $(1-\alpha)h \leqslant z \leqslant h$, are

$$p' = \left(1 - \frac{1}{\sigma}\right) c \cos\theta \tag{2.8}$$

and

$$s' = c\sin\theta + \frac{c}{\sigma} C(U-u) - 2\frac{\mu_w}{W} p, \tag{2.9}$$

respectively, where p is the particle effective pressure (total pressure minus the pore pressure), s is the particle shear stress and the presence of the sidewalls is incorporated in an average way through their coefficient μ_w of sliding friction. The balances for the particles when an upper dry layer is present can be obtained from (2.8) and (2.9) by letting σ become infinite.

In the mixture, $(1-\alpha)h \leqslant z \leqslant h$, Berzi & Jenkins (2008*a*,*b*) employed a simple constitutive relation for the fluid shear stress with a constant mixing length equal to kh:

$$S = -\frac{1-c}{\sigma} k^2 h^2 \mid U' \mid U', \tag{2.10}$$

where $k = 0.20$ (one-half Karman's constant). In the upper clear fluid layer, the constitutive relation for the fluid shear stress was again given by (2.10), with $c = 0$. Equation

(2.10) implies that large-scale turbulence develops in the flow. However, it has been suggested (Bagnold 1954) that the presence of the particles suppresses this large-scale turbulence, leaving only small-scale turbulence, with a mixing length of the order of the mean distance between the particles - roughly, one tenth of a diameter. In this case, the turbulent fluid shear stress is given by

$$S = -\frac{1-c}{100\sigma} \mid U' \mid U'; \tag{2.11}$$

while in the upper, clear fluid layer, we assume that the mixing length is proportional to the depth of the layer:

$$S = -\frac{1-c}{\sigma} k^2 (H-h)^2 \mid U' \mid U'; \tag{2.12}$$

The choice of the large- or small-scale turbulence expression influences the material parameter χ in the rheology (2.1), which has to be evaluated through fitting with experiments. Cassar *et al.* (2005) have provided some indication of when the material coefficients in the rheology (2.1) and (2.2) are the same with or without an interstitial fluid. Therefore, experimental data of the same granular material in dry and wet configurations could permit the determination of whether (2.10) or (2.11) is a suitable expression for the fluid shear stress. Such data is available for the glass spheres, used by Pouliquen (1999*b*), Jop *et al.* (2005) and Tubino & Lanzoni (1993), but, unfortunately, not for the plastic cylinders used by Armanini *et al.* (2005). It is likely, however, that the scale of the turbulence is determined by the ratio, σ, of particle density to the fluid density, i.e. by the ratio of the particle inertia to the fluid inertia. For glass spheres in water, σ is almost twice that for plastic cylinders in water. Consequently, for the latter, we will make use of (2.10), as do Berzi & Jenkins (2008*a*,*b*). Comparisons with experiments performed on glass spheres shows, however, that the choice of the scale of the turbulence does not affect the results, provided that the ratio between the particle and fluid volume fluxes is

not small (see § 3).

We make two further approximations. First, we assume that the concentration is approximately constant and at its maximum value, $c = \hat{c}$. This assumption should be regarded as the first step in an iterative process, even though the analysis on the saturated flow over an erodible bed (Berzi & Jenkins 2008*a*) shows that it is a reasonable approximation. Moreover, given that we limit the analysis to dense flows, where, as already stated, the concentration is within a relatively small range, this assumption seems plausible. Second, because the drag coefficient (2.7) is high at high concentrations, it is likely that the difference between the local particle and fluid velocity is small and, therefore, that the velocity distributions are similar; so we assume that $u' = U'$.

With these assumptions, it is possible to obtain the distribution of the particle stress ratio μ from the momentum balances (2.5), (2.6), (2.8) and (2.9) (for more details, see Berzi & Jenkins 2008*b*):

$$\mu = \frac{\sigma z + (1-\hat{c})[z - h(1-\alpha)]/\hat{c}}{\sigma z - z + h(1-\alpha)} \tan\theta + \frac{\sigma S^*}{[\sigma z - z + h(1-\alpha)]\hat{c}\cos\theta} - DI^2 - B\frac{\sigma z'^2 - [z - h(1-\alpha)]'^2}{\sigma z - z + h(1-\alpha)}, \tag{2.13}$$

where, when the flow is oversaturated, S^* is the fluid shear stress at the top of the particles. Its expression, and those of the coefficients D and B, is given in table 1. Equation (2.13) provides an illustration of the different physical mechanisms acting on the particles. The stress ratio can be seen as a measure of the mobility of the particles. The mobility of the particles is increased by the presence of the interstitial fluid, because the component of the weight in the direction parallel to the flow (the numerator in the first term on the right-hand side of 2.13) increases and, due to buoyancy, the component of the weight in the direction perpendicular to the flow (the denominator of the terms on the right-hand side of 2.13) decreases. The shear stress associated with a layer of

clear fluid above the mixture (the second term on the right-hand side of 2.13) provides additional mobility to the particles. With turbulent shear in the fluid (the third term on the right hand side of 2.13) the mobility of the particles is decreased, because less than the entire component of the fluid weight in the direction of flow contributes to the drag on the particles. Finally, the presence of frictional sidewalls (the fourth term on the right hand side of 2.13) decreases the mobility of the particles.

Using the linear rheology (2.1) in (2.12), we obtain a quadratic equation that is possible to solve for I as a function of z. Once this distribution is known, it is possible to derive the variation of μ with z, given in table 1, and the distribution of the particle shear rate in the flowing layer. Given the definition of the inertial parameter and the constitutive relations, we may also calculate the location, ζ, of the base of the plug, the value of the particle velocity, u_p, there, and the mean value, u_m, of the particle velocity in the flowing layer ($\zeta \leqslant z \leqslant h$). All of these results are reported in table 1. In the following, we extend these relations in order to take into account the possible presence of an upper, dry, sheared layer above the plug and a non-zero slip-velocity, u_b, at a rigid base.

With $u' = U'$, the difference between the value of the fluid velocity, U_p, at $z = \zeta$ and the mean value, U_m, of the fluid velocity in the flowing layer ($\zeta \leqslant z \leqslant h$) and the corresponding values for the particles is constant. However, this implies that the fluid would slip over the rigid bed. Consequently, we regard the theory to apply everywhere except in a boundary layer close to the rigid bed, where the fluid velocity goes to zero and the particle velocity goes to a finite non-zero value. In order to evaluate the constant difference δu between the fluid and the particle velocity above this boundary layer, we make use of the balance (2.6) at its top, $z \approx h$:

$$\frac{\hat{c}}{\sigma(1-\hat{c})^{3.1}}\left(\frac{3}{10} \mid \delta u \mid + \frac{18.3}{R}\right)\delta u = \Delta, \tag{2.14}$$

where $\Delta = (1-\hat{c})\sin\theta/\sigma - S'(h)$ is the difference between the component of the fluid weight in the direction parallel to the flow and the internal resistance due to the fluid shear stress, evaluated at $z \approx h$. The quantity $S'(h)$ can easily be obtained from the constitutive relation (2.10) or (2.12), given the distribution of $U' = u'$ along z (see table 1). Depending on whether Δ is positive or negative, the fluid is either faster or slower than the particles. For flow over an erodible bed, we have assumed (Berzi & Jenkins 2008*a*,*b*) that the fluid shear stress at its surface is zero. Then, (2.14) reduces to the classical equation governing flows through a porous bed (de Marsily 1981) and the fluid is always faster than the particles. The general solution of (2.14) is:

$$\delta u = \left\{ -\frac{18.3}{0.6R} + \frac{1}{2}\left[\left(\frac{18.3}{0.3R} \right)^2 + \frac{4\sigma(1-\hat{c})^{3.1} \mid \Delta \mid}{0.3\hat{c}} \right]^{1/2} \right\} \frac{\Delta}{\mid \Delta \mid}. \tag{2.15}$$

The value of the mean velocity, U_{cm}, in the upper, clear-fluid layer, $h(1-\beta) \leqslant z \leqslant 0$, present only in the over-saturated case, can also be evaluated using (2.10) or (2.12) in (2.6), upon taking c = 0 and integrating twice. The result, already given in Berzi & Jenkins (2008*b*) for the case of large-scale turbulence, is also reported in table 1.

In table 2 we provide the corresponding results for a channel of infinite width - that is, for a channel with no sidewalls. The results for this case can not be obtained in general by simply taking $\mu_w = 0$ in the expressions of table 1, because the coefficient B that contains the wall friction coefficient multiplies the highest power of z in (2.13) (see the Appendix A for more details).

2.2. *Upper, dry, shear layer*

In the upper, dry layer of an under-saturated flow, the ratio of shear stress to pressure is, with the assumption of constant concentration,

$$\mu = \tan\theta - \frac{\mu_w}{W} z, \tag{2.16}$$

$$
\begin{aligned}
\mu &= \breve{\mu} + \chi\left\{-\chi/2D + (BD)^{1/2}(-z^2+2Fz+N)^{1/2}/[D(z+L)^{1/2}]\right\}\\
u' &= \chi\left[(1-1/\sigma)\cos\theta\right]^{1/2}(z+L)^{1/2}/2D - \left[B\,(1-1/\sigma)\cos\theta/\,D\right]^{1/2}(-z^2+2Fz+N)^{1/2}\\
A &= \lfloor\sigma + (1-\hat{c})/\hat{c}\rfloor\tan\theta/(\sigma-1) - \breve{\mu}\\
B &= \mu_w/W\\
D &= k^2h^2\xi^2(1-\hat{c})/(\sigma\hat{c}) \text{ (large scale turbulence) or}\\
D &= (1-\hat{c})/(100\sigma\hat{c}) \text{ (small scale turbulence)}\\
F &= (\chi^2+4AD)/(8BD) - L\\
L &= h(1-\alpha)/(\sigma-1)\\
N &= L\left[\chi^2/(4D) - (1-\hat{c})\tan\theta/\hat{c} - \breve{\mu} + BL(\sigma-1)\right]/B + \sigma S^*/\left[(\sigma-1)B\hat{c}\cos\theta\right]\\
S^* &= h\sin\theta(\beta-1)/\sigma\\
\zeta &= -\left[\chi^2/(4BD) - 2F\right]/2 - \left\{\left[\chi^2/(4BD)-2F\right]^2 - 4\left[\chi^2L/(4BD)-N\right]\right\}^{1/2}/2\\
u_m &= u_b - \chi\left[(1-1/\sigma)\cos\theta\right]^{1/2}\left\{(h+L)^{3/2}(h-\zeta)\right.\\
&- \left.\tfrac{2}{5}\left[(h+L)^{5/2} - (\zeta+L)^{5/2}\right]\right\}/[3D(h-\zeta)]\\
&+ \left[BD\,(1-1/\sigma)\cos\theta\right]^{1/2}\left\{(h-F)\left(2Fh-h^2+N\right)^{1/2}\right.\\
&+ \left.(F^2+N)\sin^{-1}\left[(h-F)/\left(F^2+N\right)^{1/2}\right]\right\}/(2D)\\
&- \left[BD\,(1-1/\sigma)\cos\theta\right]^{1/2}\left\{-\tfrac{1}{3}\left(2Fh-h^2+N\right)^{3/2} + \tfrac{1}{3}\left(2F\zeta-\zeta^2+N\right)^{3/2}\right.\\
&+ \left(F^2+N\right)^{3/2}\left[(h-F)\sin^{-1}\left((h-F)/\left(F^2+N\right)^{1/2}\right)/\left(F^2+N\right)^{1/2}\right.\\
&- \left.(\zeta-F)\sin^{-1}\left((\zeta-F)/\left(F^2+N\right)^{1/2}\right)/\left(F^2+N\right)^{1/2}\right.\\
&+ \left.\left.\left(1-(h-F)^2/(F^2+N)\right)^{1/2} - \left(1-(\zeta-F)^2/\left(F^2+N\right)\right)^{1/2}\right]\right\}/[2D(h-\zeta)]\\
u_p &= u_b - \chi[(1-1/\sigma)\cos\theta]^{1/2}\left[(h+L)^{3/2} - (\zeta+L)^{3/2}\right]/(3D)\\
&- \left[BD\,(1-1/\sigma)\cos\theta\right]^{1/2}\left\{(\zeta-F)\left(2F\zeta-\zeta^2+N\right)^{1/2}\right.\\
&+ \left.\left(F^2+N\right)\sin^{-1}\left[(\zeta-F)/\left(F^2+N\right)^{1/2}\right]\right\}/(2D)\\
&+ \left[BD\,(1-1/\sigma)\cos\theta\right]^{1/2}\left\{(h-F)\left(2Fh-h^2+N\right)^{1/2}\right.\\
&+ \left.\left(F^2+N\right)\sin^{-1}\left[(h-F)/\left(F^2+N\right)^{1/2}\right]\right\}/(2D)\\
U_m &= u_m + \delta u\\
U_p &= u_p + \delta u\\
U_{cm} &= U_p + 2(h\sin\theta)^{1/2}(\beta-1)^{3/2}/(5k\beta) \text{ (large scale turbulence) or}\\
U_{cm} &= U_p + 2(h\sin\theta)^{1/2}(\beta-1)^{1/2}/(5k) \text{ (small scale turbulence)}
\end{aligned}
$$

TABLE 1. Summary of the results for steady, uniform flows between frictional sidewalls.

$$
\begin{aligned}
\mu &= \breve{\mu} + \chi\left\{-\chi/2D + (2Fz+N)^{1/2}/[D(z+L)]^{1/2}\right\}\\
u' &= \chi\left[(1-1/\sigma)\cos\theta\right]^{1/2}(z+L)^{1/2}/2D - \left[(1-1/\sigma)\cos\theta/\,D\right]^{1/2}(2Fz+N)^{1/2}\\
F &= (\chi^2+4AD)/(8D)\\
N &= L\left[\chi^2/(4D) - (1-\hat{c})\tan\theta/\hat{c} - \breve{\mu}\right] + \sigma S^*/\left[(\sigma-1)\hat{c}\cos\theta\right]\\
\zeta &= \left(4DN-\chi^2 L\right)/\left(\chi^2-8DF\right)\\
u_m &= u_b - \chi\left[(1-1/\sigma)\cos\theta\right]^{1/2}\left\{(h+L)^{3/2}(h-\zeta)\right.\\
&- \left.\tfrac{2}{5}\left[(h+L)^{5/2}-(\zeta+L)^{5/2}\right]\right\}/[3D(h-\zeta)]\\
&- \left[(1-1/\sigma)\cos\theta\right]^{1/2}\Big[(2Fh+N)^{5/2}-(2F\zeta+N)^{5/2}\\
&- 5F(2Fh+N)^{3/2}(h-\zeta)\Big]/\left[15D^{1/2}F^2(h-\zeta)\right]\\
u_p &= u_b - \chi\left[(1-1/\sigma)\cos\theta\right]^{1/2}\left[(h+L)^{3/2}-(\zeta+L)^{3/2}\right]/(3D)\\
&- \left[(1-1/\sigma)\cos\theta\right]^{1/2}\left[(2F\zeta+N)^{3/2}-(2Fh+N)^{3/2}\right]/\left(3FD^{1/2}\right)
\end{aligned}
$$

TABLE 2. Summary of the results for steady, uniform flows without sidewalls. Only expressions different from those of table 1 are shown.

as in the case of a dry granular flow between frictional sidewalls investigated by Jop *et al.* (2005). The stress ratio μ is proportional to the inertial parameter and it must exceeds its minimum value $\breve{\mu}$ to have a non-zero I. If $\tan\theta < \breve{\mu}$, then, for $0 \leqslant z \leqslant \zeta$, the shear rate is zero (a plug); if, instead, $\tan\theta > \breve{\mu}$, then a part of the dry layer of thickness $h(1-\alpha)$ is subject to shearing. Upon taking $\mu = \breve{\mu}$ in (2.16), we can determine the thickness ψ of this shear layer:

$$\psi = \min\left[(\tan\theta - \breve{\mu})\,W/\mu_w, h(1-\alpha)\right]. \tag{2.17}$$

Equation (2.17) accounts for the fact that the thickness ψ must be, at most, equal to the total extent of the dry layer. In the dry shear layer, $0 \leqslant z \leqslant \psi$, we can employ the linear rheology (2.1) in (2.16), the definition of the inertial parameter and the pressure

distribution $p = \hat{c}z\cos\theta$ (from 2.8, with the density ratio σ infinite) to obtain

$$u' = -\frac{(\cos\theta)^{1/2}}{\chi}\left[(\tan\theta - \check{\mu})z^{1/2} - \frac{\mu_w}{W}z^{3/2}\right]. \tag{2.18}$$

Upon integrating twice between 0 and ψ and using the boundary condition $u(\psi) = u_p$, we obtain the mean value of the particle velocity in the dry shear layer:

$$u_\psi = \frac{(\cos\theta)^{1/2}}{\chi}\psi^{3/2}\left[\frac{2}{5}(\tan\theta - \check{\mu}) - \frac{2}{7}\mu_w\psi/W\right] + u_p. \tag{2.19}$$

This expression includes dry granular flow as a special case.

2.3. *Slip velocity at the base*

We next extend the theory to accommodate a non-zero slip velocity u_b at a rigid, bumpy bed. We assume that the inertia of the particles is great enough so that the presence of the fluid does not affect the particle interactions. Then, we can make use of previous work on boundary conditions for dry collisional granular flows over a rigid, bumpy base (Richman 1988; Jenkins 2001). The main result is that at the boundary there is a relation between the value of the particle stress ratio μ_b and the quantity $u_b/(p_b/c_b)^{1/2}$, where p_b and c_b are the particle pressure and concentration at the boundary. This relation can be interpreted as the rheology of the boundary. The term $u_b/(p_b/c_b)^{1/2}$ is the inertial number at the bed, with the role of the shear rate taken by the ratio of the slip velocity to the particle diameter.

Upon taking $z = h$, we may obtain, from the distribution of μ in table 1 or table 2, the value of the particle stress ratio at the bed:

$$\mu_b = \mu(h). \tag{2.20}$$

If the flow is over an erodible bed, $\mu_b = \check{\mu}$, and (2.20) provides a relation between the height of the particles and the inclination of the bed.

Finally, we assume here that the stress ratio at the bed can be expressed as:

$$\mu_b = \breve{\mu} + \chi \frac{u_b}{(1-\alpha/\sigma)^{1/2}(h\cos\theta)^{1/2}}, \tag{2.21}$$

where we have taken $c_b = \hat{c}$ and $p_b = (1-\alpha/\sigma)h\hat{c}\cos\theta$. Boundary conditions derived using arguments from the kinetic theory for rigid flat walls to which frictional spheres have been attached have this form (Jenkins 2001). Here, rather than adopting the coefficients calculated using kinetic theories, we assume that the coefficients are the same as those of (2.1). In this case, (2.21) provides continuity with the solution over an erodible bed (Berzi & Jenkins 2008*b*), given that when $\mu_b = \breve{\mu}$, the slip velocity is equal to zero.

We can now evaluate the volume flux of particles per unit width,

$$q = \hat{c}u_m(h-\zeta) + \hat{c}u_p(\zeta-\psi) + \hat{c}u_\psi\psi, \tag{2.22}$$

and the volume flux of fluid per unit width,

$$Q = (1-\hat{c})U_m(h-\zeta) + (1-\hat{c})U_p\left[\zeta - h(1-\alpha)\right] + U_{cm}h(\beta-1), \tag{2.23}$$

or, equivalently, the average particle velocity:

$$u_A = \frac{q}{\hat{c}h}, \tag{2.24}$$

and the average fluid velocity:

$$U_A = \frac{Q}{h\left[\beta - 1 + \alpha(1-\hat{c})\right]}. \tag{2.25}$$

In conclusion, the four governing equations (2.20), (2.21), (2.22) and (2.23) constrain seven variables q, Q, u_b, h, ξ, μ_b and θ. That is, there are three degrees of freedom for a steady, fully developed flow of a granular–fluid mixture over a rigid bed. For example, we can specify the particle and fluid volume fluxes and the angle of inclination of the rigid bed, and determine the remaining variables from the governing equations. For a flow over an erodible bed, we have the additional condition $\mu_b = \breve{\mu}$, so that there are only two degrees of freedom. Once the particle and fluid volume fluxes are specified, the angle of

inclination of the erodible bed, equal to that of the free surface, is determined as part of the solution. Alternatively, we could specify the average velocity u_A (or U_A), h and ξ and obtain the remaining variables, in particular the angle of inclination θ, from the governing equations. We will use this approach to deal with steady, non-uniform flows.

2.4. *Limitations of the theory*

We expect the theory to describe steady, uniform, thick, dense flows of a granular–fluid mixture in relatively wide rectangular channels with frictional sidewalls in which the Stokes number in most of the flow exceeds unity. As already stated, a thickness of at least 10 particle diameters is required to disregard the influence of boundaries. For thick flows, this prevents the prediction of realistic concentration distribution close to the free surface and the bed. For flows of, roughly, 15 particle diameters and less in width, we anticipate that fluid forces associated with shearing across the flow, due to the no-slip condition at the side walls, become important. The limitation on the Stokes number is required because we use a definition of the inertial parameter valid when the time scale associated with free-fall motion of particles is much shorter than the time scale associated with the viscous drag (Cassar *et al.* 2005).

The limitation to dense flows, for which we expect rheology (2.1) be valid, deserves additional consideration. As already stated, the rheology of (2.1) and (2.2) provides ranges for the inertial parameter ($0 \leqslant I \leqslant \hat{I}$) and for the stress ratio ($\check{\mu} \leqslant \mu \leqslant \hat{\mu}$), given a range of concentration ($\check{c} \leqslant c \leqslant \hat{c}$) for the flows that we consider as dense, i.e. those for which correlated motion between the particles is present (Jenkins 2006, 2007). Actually, the minimum value of I, corresponding to the minimum value of the stress ratio at the interface with an erodible bed or a plug, would not be exactly zero, because the bed creeps (Komatsu *et al.* 2001). However, the creeping flow is so slow that it makes a negligible contribution to the volume flux on the usual time scale of laboratory experiments; so we

do not expect this approximation have a large influence on the predictions. Quantitative evaluation of the range of the parameters I, μ, and c requires knowledge of the material coefficients in the particle rheology. The range of parameters for the granular material used by Armanini *et al.* (2005) and Larcher *et al.* (2007) in their experiments, to which the present theory has been compared in Berzi & Jenkins (2008*a*,*b*), will be provided in the following section. However, as an example, in the numerical simulations performed by Mitarai & Nakanishi (2007) on simple shear flow of frictionless spheres, over the range of concentration $0.5 \leqslant c \leqslant 0.6$, the range of particle stress ratio was $0.30 \leqslant \mu \leqslant 0.53$.

Once the upper limit of the stress ratio $\hat{\mu}$ is known, we can use this information to bound the analytical solutions for dense flows. For a flow between frictional sidewalls, we have determined the distribution of the stress ratio with z. In the upper dry granular layer it is given by (2.16); and, for $\zeta \leqslant z \leqslant h$, is reported in table 1. This distribution is characterised by a maximum at $z = 0$. This maximum is infinite for an over-saturated flow, because the particle pressure is zero and the particle shear stress is finite, because of the shear stress exerted on the particles by the clear fluid above. Consequently, the theory can describe an over-saturated flow, except for a boundary layer at the interface with the clear fluid. To include over-saturated flows, we assume that in any kind of flow, the maximum value, μ_M, of the stress ratio occurs at $z = 1$. That is, the maximum stress ratio in the flow is below the first layer of particles and can be evaluated from the distribution of μ reported in table 1.

When the upper, dry layer is entirely sheared in an under-saturated flow, μ_M is, therefore, equal to $\tan\theta - \mu_w/W$ (from 2.16), otherwise there is also a local maximum for μ in the region $\zeta \leqslant z \leqslant h$, whose position can be determined from $\mathrm{d}\mu/\mathrm{d}z = 0$ with $\mu(z)$ given in table 1. The implication is that the theory applies when the tangent of the angle of inclination of the free-surface is less than $\hat{\mu} + \mu_w/W$. We will see in the next section that,

given a fixed volume flux of fluid, this corresponds to a maximum volume flux of particles (or equivalently to a minimum degree of saturation ξ). On the other hand, we will also see that, given the same volume flux of fluid, the upper limit of μ in an over-saturated flow implies a minimum volume flux of particles (or equivalently, a maximum degree of saturation) for having a dense flow.

2.5. *Steady, non-uniform, flow*

We now extend the analysis outlined in the previous sections to describe the propagation of a steady wave of a granular–fluid mixture over a rigid, bumpy bed. This particular flow configuration has been experimentally investigated by Davies (1988) and seems to possess some features in common with natural debris flows. Consequently, it represents a realistic test of the present theory for its possible practical applications.

A sketch of the flow configuration with the frame of reference is depicted in figure 2. In contrast to figure 1, the origin of the Z-axis is at the rigid bed and the coordinate Z increases towards the free surface. The origin of the x-axis is taken to be somewhere upslope. Both the particle and the fluid depth are functions of x, with x^* and X^* indicating the position of the particle and fluid snout, respectively. At each value of x, the ratio H/h can be greater than, equal to, or less than unity (over-, fully and under-saturated flow); also, either h or H can vanish (clear fluid or dry granular flow).In the following, we focus on the governing equations for the part of the wave in which both particles and fluid are present, $x <\min(x^*, X^*)$, and defer the analysis of the front to the next sub-section.

The longitudinal momentum balance for the fluid is:

$$\frac{1}{\sigma}\frac{\mathrm{d}U}{\mathrm{d}t} = \frac{1}{\sigma}\sin\phi + \frac{\partial S}{\partial Z} - \frac{\partial P}{\partial x}, \tag{2.26}$$

if $h \leqslant Z \leqslant \beta h$, or

$$\frac{1-c}{\sigma}\frac{\mathrm{d}U}{\mathrm{d}t} = \frac{1-c}{\sigma}\sin\phi - \frac{c}{\sigma}C(U-u) + \frac{\partial S}{\partial Z} - \frac{\partial (1-c)P}{\partial x} - P\frac{\partial c}{\partial x}, \tag{2.27}$$

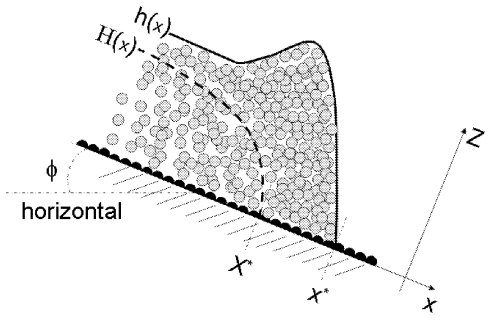

FIGURE 2. Frame of reference used for the analysis of a steady, non-uniform flow over a rigid bumpy bed.

if $0 \leqslant Z \leqslant \alpha h$, where we recall that when $\xi \equiv H/h \leqslant 1$, $\alpha = \xi$ and $\beta = 1$, and the term involving the gradient of concentration along the flow accounts for the buoyancy of the particles in the way suggested by Drew & Passman (1999). The longitudinal momentum balance for the particles is:

$$c\frac{\mathrm{d}u}{\mathrm{d}t} = c\sin\phi - 2\frac{\mu_w}{W}p + \frac{\partial s}{\partial Z} - \frac{\partial p}{\partial x}, \tag{2.28}$$

if $\alpha h \leqslant Z \leqslant h$, or

$$c\frac{\mathrm{d}u}{\mathrm{d}t} = c\sin\phi + \frac{c}{\sigma}C(U-u) - 2\frac{\mu_w}{W}p + \frac{\partial s}{\partial Z} - \frac{\partial (p+cP)}{\partial x} + P\frac{\partial c}{\partial x}, \tag{2.29}$$

if $0 \leqslant Z \leqslant \alpha h$, where $p + cP$ represents the total particle pressure. When the inertial terms $\mathrm{d}U/\mathrm{d}t$ and $\mathrm{d}u/\mathrm{d}t$ and the non-uniformity in the x-direction vanish, and $\phi = \theta$, (2.26)-(2.27) and (2.28)-(2.29) reduce to (2.6) and (2.9).

Depth-averaging the longitudinal momentum balances (2.26)-(2.27) and (2.28)-(2.29), with concentration constant and equal to $\hat{c}$, gives, for the fluid and the particles, respectively,

$$\begin{aligned}[\beta - 1 + \alpha(1-\hat{c})]\, h\frac{\mathrm{d}U_A}{\mathrm{d}t} = \frac{\beta - 1 + \alpha(1-\hat{c})}{\sigma}h\sin\phi - \frac{\hat{c}}{\sigma}\int_0^{\alpha h} C(U-u)\mathrm{d}Z + \int_0^{\xi h}\frac{\partial S}{\partial Z}\mathrm{d}Z \\ -(1-\hat{c})\int_0^{\alpha h}\frac{\partial P}{\partial x}\mathrm{d}Z - \int_h^{\beta h}\frac{\partial P}{\partial x}\mathrm{d}Z\end{aligned} \tag{2.30}$$

and

$$\hat{c}h\frac{\mathrm{d}u_A}{\mathrm{d}t} = \hat{c}h\sin\phi + \frac{\hat{c}}{\sigma}\int_0^{\alpha h} C(U-u)\mathrm{d}Z - \int_0^h 2\frac{\mu_w}{W}p\mathrm{d}Z + \int_0^h \frac{\partial s}{\partial Z}\mathrm{d}Z - \int_0^h \frac{\partial p}{\partial x}\mathrm{d}Z - \hat{c}\int_0^{\alpha h}\frac{\partial P}{\partial x}\mathrm{d}Z, \tag{2.31}$$

where,

$$\frac{\mathrm{d}U_A}{\mathrm{d}t} \equiv \frac{1}{[\beta - 1 + \alpha(1-\hat{c})]\,h}\left[\int_h^{\beta h}\frac{\mathrm{d}U}{\mathrm{d}t}\mathrm{d}Z + (1-\hat{c})\int_0^{\alpha h}\frac{\mathrm{d}U}{\mathrm{d}t}\mathrm{d}Z\right] \tag{2.32}$$

and

$$\frac{\mathrm{d}u_A}{\mathrm{d}t} \equiv \frac{1}{h}\int_0^h \frac{\mathrm{d}u}{\mathrm{d}t}\mathrm{d}Z. \tag{2.33}$$

Equations (2.32) and (2.33) are formally derived in Appendix B.

We now make the fundamental assumption that the resistances due to the internal shear stresses, the sidewalls, and the drag force in (2.30) and (2.31) can be approximated by the expressions valid when the flow is steady and uniform, i.e. when they balance only the component of the particle weight in the x-direction:

$$\frac{\hat{c}}{\sigma}\int_0^{\alpha h} C(U-u)\mathrm{d}Z - \int_0^{\xi h}\frac{\partial S}{\partial Z}\mathrm{d}Z = \frac{1}{\sigma}\left[\beta - 1 + \alpha(1-\hat{c})\right]h\sin\Theta \tag{2.34}$$

and

$$-\frac{\hat{c}}{\sigma}\int_0^{\alpha h} C(U-u)\mathrm{d}Z + \int_0^h 2\frac{\mu_w}{W}p\mathrm{d}Z - \int_0^h \frac{\partial s}{\partial Z}\mathrm{d}Z = \hat{c}h\sin\theta. \tag{2.35}$$

The angles Θ and θ coincide with the inclination of the bed in a steady, uniform flow. However, in the steady, non-uniform flow considered here, these three angles are different: the inclination ϕ of the rigid, bumpy bed is known, while Θ and θ can be evaluated from the solutions for the steady, uniform flows summarized in tables 1 and 2 using the local values of the non-uniform heights. That is, we specify u_A and U_A. Then, as indicated at the end of the sub-section on the slip velocity at the base, the specification of u_A, h and ξ results in a value of θ that, in general, is different from ϕ. Similarly, the specification of U_A results in an inclination Θ different from both ϕ and θ. The angles agree if the

depths of the fluid and particles become equal to their uniform values.

The use of the resistance of a steady, uniform flow in a higher order unsteady, non-uniform momentum equation is of common use in hydraulics (Chow 1959) and has already been employed to describe the steady, non-uniform motion of dry granular flows (Pouliquen 1999*a*) and debris flows (Hungr 2000).

Using Leibniz's rule, we may write the non-uniform terms in (2.30) and (2.31) as

$$\int_0^{\alpha h} \frac{\partial P}{\partial x} \mathrm{d}Z = \frac{\partial}{\partial x} \int_0^{\alpha h} P \mathrm{d}Z - P \mid_{Z=\alpha h} \frac{\partial(\alpha h)}{\partial x}, \tag{2.36}$$

$$\int_h^{\beta h} \frac{\partial P}{\partial x} \mathrm{d}Z = \frac{\partial}{\partial x} \int_h^{\beta h} P \mathrm{d}Z + P \mid_{Z=h} \frac{\partial h}{\partial x} \tag{2.37}$$

and

$$\int_0^{h} \frac{\partial p}{\partial x} \mathrm{d}Z = \frac{\partial}{\partial x} \int_0^{h} p \mathrm{d}Z, \tag{2.38}$$

respectively. Equations (2.36)-(2.38) account for the vanishing of the fluid and particle pressure at $Z = \beta h$ and $Z = h$, respectively, and for the fact that the bed is a rigid boundary (i.e. they describe the non-erosional, non-depositional nature of the flow - that is, no erodible bed is allowed to develop).

To close the problem, we require an expression for the distribution of the fluid and particle pressure in the flow. Assuming that the length of the wave is much greater than its depth (the shallow-water assumption), we can obtain the distribution of P and p in the Z-direction by integrating (2.5) and (2.8), replacing θ by ϕ, and using the boundary conditions $P(H) = 0$ and $p(h) = 0$:

$$P = \frac{1}{\sigma}(H - Z)\cos\phi, \tag{2.39}$$

and

$$p = (h - Z)\hat{c}\cos\phi, \tag{2.40}$$

if $\alpha h \leqslant Z \leqslant h$, or

$$p = h(1-\alpha)\hat{c}\cos\phi + (\alpha h - Z)(\sigma - 1)\hat{c}\cos\phi/\sigma, \tag{2.41}$$

if $0 \leqslant Z \leqslant \alpha h$. Then, upon employing (2.39) and (2.40)-(2.41) in (2.36)-(2.38), we obtain:

$$\frac{\partial}{\partial x}\int_0^{\alpha h} P\mathrm{d}Z - P\mid_{Z=\alpha h}\frac{\partial(\alpha h)}{\partial x} = \frac{\alpha h}{\sigma}\cos\phi\frac{\partial H}{\partial x}, \tag{2.42}$$

$$\frac{\partial}{\partial x}\int_h^{\beta h} P\mathrm{d}Z + P\mid_{Z=h}\frac{\partial h}{\partial x} = \frac{\beta h - h}{\sigma}\cos\phi\frac{\partial H}{\partial x} \tag{2.43}$$

and

$$\frac{\partial}{\partial x}\int_0^h p\mathrm{d}Z = h\left(1-\alpha^2/\sigma\right)^{1/2}\hat{c}\cos\phi\frac{\partial}{\partial x}\left[h\left(1-\alpha^2/\sigma\right)^{1/2}\right]. \tag{2.44}$$

The steady, non-uniform flow, sometimes referred to as a uniform progressive wave, is characterized by the fact that u_A and U_A are equal and independent of x (Hungr 2000). This implies $\mathrm{d}U_A/\mathrm{d}t = \mathrm{d}u_A/\mathrm{d}t = 0$ and, using (2.34)-(2.38) and (2.42)-(2.44), (2.30) and (2.31) reduce to:

$$\frac{\mathrm{d}H}{\mathrm{d}x} = \tan\phi - \frac{\sin\Theta}{\cos\phi} \tag{2.45}$$

and

$$\left(1-\frac{\alpha}{\sigma}\right)\frac{\mathrm{d}h}{\mathrm{d}x} + \frac{\alpha}{\sigma}\frac{\mathrm{d}(\beta h)}{\mathrm{d}x} = \tan\phi - \frac{\sin\theta}{\cos\phi}. \tag{2.46}$$

Equations (2.45) and (2.46) can be further simplified if we assume that the angles ϕ, θ,and Θ are small:

$$\frac{\mathrm{d}H}{\mathrm{d}x} = \tan\phi - \tan\Theta \tag{2.47}$$

and

$$\left(1-\frac{\alpha}{\sigma}\right)\frac{\mathrm{d}h}{\mathrm{d}x} + \frac{\alpha}{\sigma}\frac{\mathrm{d}(\beta h)}{\mathrm{d}x} = \tan\phi - \tan\theta. \tag{2.48}$$

Solutions of the two ordinary differential equations (2.47) and (2.48) provide the evolution of depths $h(x)$ and $H(x)$, when both particles and fluid are present, $x < \min(x^*, X^*)$, once the value of the angle of inclination of the rigid bumpy bed, ϕ, the common value

of the average velocities, $u_A = U_A$, and two boundary conditions are specified. The two boundary conditions are the values of h and H at $x = \min(x^*, X^*)$. In the following sub-section we show how we set these boundary conditions.

2.6. *Wave front*

The natural boundary conditions at the snouts are the vanishing of the particle and fluid depths, i.e. $h(x^*) = 0$ and $H(X^*) = 0$. This poses a problem, because we are using the results of a theory on steady, uniform flows to approximate the resistances in a non-uniform situation; we have already emphasized that the theory does not apply when the flow is thin. In addition, near the snouts, the inertial terms in the normal momentum balances are not negligible, so that the shallow-water assumption also fails (the distribution of pressures is not hydrostatic) and (2.47) and (2.48) do not provide a faithful description of the phenomenon. Nonetheless, we accept these drawbacks as part of the approximations of the theory and describe the snouts in the context of the model (Hunt 1984, 1994). In the following, we consider, for simplicity, situations in which the influence of the sidewalls is negligible (i.e., $\mu_w = 0$), as in the experiments performed by Davies (1988) (see the next section). The extension to situations in which sidewalls are present is straightforward.

In general, x^* is different from X^*, so that the front of the wave could be either a clear fluid ($x^* < X^*$) or dry ($x^* > X^*$). Davies' (1988) careful qualitative description of his experiments refers to steady waves with a dry front. Consequently, we limit our analysis to this case.

If the front is dry, then, for $X^* \leqslant x \leqslant x^*$, $H = 0$; while h evolves according to:

$$\frac{\mathrm{d}h}{\mathrm{d}x} = \tan\phi - \tan\theta. \tag{2.49}$$

In this simple case, we can obtain $\tan\theta$ as an explicit function of u_A and h from the solution for a steady, uniform, dry flow. Using (2.19) and (2.21), with $u_\psi = u_A$, $\psi = h$, $u_p = u_b$, $\sigma = \infty$, $\cos\theta \approx 1$ and $\mu_b = \mu = \tan\theta$ (from 2.16, with $\mu_w = 0$),

$$\tan\theta = \check{\mu} + \chi \frac{u_A}{(2h/5+1)h^{1/2}}. \tag{2.50}$$

Equation (2.49) implies that, for a dry front, $\mathrm{d}h/\mathrm{d}x$ must be negative at $x = x^*$, where $h = 0$. Given that the stress ratio is constant and equal to $\tan\theta$ and that we can have a dense flow when $\check{\mu} \leqslant \mu \leqslant \hat{\mu}$, this condition constrains the angle of inclination of the rigid bed ($\check{\mu} \leqslant \tan\phi \leqslant \hat{\mu}$). It implies that it is not possible to have a steady wave with a dry granular front, if the angle of inclination of the rigid bed is less than the angle of repose of the granular material (about 22° for the plastic cylinders used by Armanini *et al.* (2005), as stated in the next section). Davies (1988) experiments were performed at angles of inclination of the rigid bed less than 19° with somewhat different particles than those employed by Armanini *et al.* (2005). The low values of the angles of inclination may indicate that the extremely simplified rheology of the boundary that we adopt is unrealistic. We note that in Davies' (1988) experiments, the dense granular–fluid flow developed over a thin collisional basal layer, so that a more detailed analysis of the boundary, e.g. that performed by Jenkins & Askari (1999), might be more suitable.

Equation (2.49) with (2.50) can be easily integrated for $X^* \leqslant x \leqslant x^*$. The value of $h = h^*$ at $x = X^*$ can then be used as a boundary condition, together with $H(X^*) = 0$, to solve (2.47) and (2.48). We use $\tan\Theta = \check{\mu} + \chi(U_A - \delta u)h^{*-1/2}$ for $H(X^*) = 0$ in (2.47), from (2.21), with $\mu_b = \tan\Theta$ and $u_b = U_A - \delta u$, where δu is a function of the square root of $\tan\Theta$ (equation 2.14, replacing θ by Θ in the expression for Δ, with $S' = 0$).

The control parameters in the problem are the inclination ϕ of the rigid bumpy bed, the common value of the average velocities $u_A = U_A$ (necessary, together with H and h, to evaluate $\tan\theta$ and $\tan\Theta$ at every step of the integration) and the positions x^* and X^*

of the snouts. Equivalently, the latter two control parameters can be replaced by

$$V = \int_0^{X^*} \left[\beta - 1 + \alpha(1 - \hat{c})\right] h \mathrm{d}x \tag{2.51}$$

and

$$v = \hat{c} \int_0^{x^*} h \mathrm{d}x; \tag{2.52}$$

these are, respectively, the total volume per unit width of the fluid and particles contained in the wave between its snout and the origin of the x-axis.

In the following section, we provide the results of the theoretical treatment outlined above and test the predictions of the theory against existing experiments.

3. Applications

3.1. *Steady, uniform, flow*

Here, we present features of the analytical solutions for a mixture of water ($\rho = 1000\,\mathrm{kg/m^3}$ and $\eta = 10^{-3}\,\mathrm{Pa \cdot s}$) and plastic cylinders ($\sigma = 1.54$ and equivalent spherical diameter $d = 0.0037$ m). These particles have been used by Armanini *et al.* (2005) and Larcher *et al.* (2007) to investigate steady, fully developed particle–fluid flows over both rigid and erodible beds. Previously (Berzi & Jenkins 2008*a*,*b*), we indicated the capability of the present theory to reproduce the experiments of Armanini *et al.* (2005) for the flows over an erodible bed. We employ here the same values of the coefficients in the particle rheology and the wall friction: $\check{\mu} = 0.41$, $\chi = 0.5$, $\hat{c} = 0.69$, $b = 0.3$ and $\mu_w = 0.27$. We also assume that dense flows of these non-spherical particles take place within the concentration range 0.55 to 0.69; the lowest value of concentration implies $\hat{\mu} = 0.64$. We provide the value of b even though in our approximate solution we will not make use of (2.2) to solve for the concentration distribution.

Quantitative comparisons are also made with the experiments on dry granular flows of

glass spheres ($d = 0.005$ m) over a rigid bed without sidewalls by Pouliquen (1999*b*) and over an erodible bed between sidewalls made of glass by Jop *et al.* (2005), and with the experiments on the steady, uniform flow of a mixture of water and glass spheres ($\sigma = 2.60$ and $d = 0.003$ m) over an erodible bed between sidewalls made of polycarbonate by Tubino & Lanzoni (1993). For glass spheres we use $\check{\mu} = 0.38$ and $\hat{\mu} = 0.64$ (as suggested by Pouliquen (1999*b*)), $\chi = 0.6$, $\hat{c} = 0.6$ and $\mu_w = 0.22$.

When the flow is not dry, we solve for the flow behaviour by changing the particle flux while keeping the fluid flux constant. This, at least in principle, can be done in the physical experiments. Because of the implicit nature of the expressions reported on in tables 1 and 2, we first set the degree of saturation $\xi \equiv H/h$, on which the coefficients α and β depend; then, through an iterative process implemented in MATLAB using the built-in function FZERO, we find the value of h that satisfies the condition on the fluid flux. With ξ and h, all of the other quantities can be obtained explicitly using the relations provided in tables 1 and 2. As previously stated, the value of $\tan\theta$ coincides with the slope of the bed for flow over a rigid bed, while is a function of h for flows over an erodible bed (obtained by replacing h and $\check{\mu}$ by z and μ, respectively, in the first expression of table 1).

First, we make quantitative comparisons with existing experimental data to assess the validity of the present theory for different flow configurations. Then, we carry out a careful analysis of the capability of the present theory to explain key features observed in steady, uniform granular–fluid flows and make some predictions that will have to be tested in experiments.

In figure 3, we show the comparisons between the results of the present theory and experiments performed on dry granular flows of glass spheres. Figure 3a depicts the average particle velocity versus the particle depth for the flow on an incline in absence of

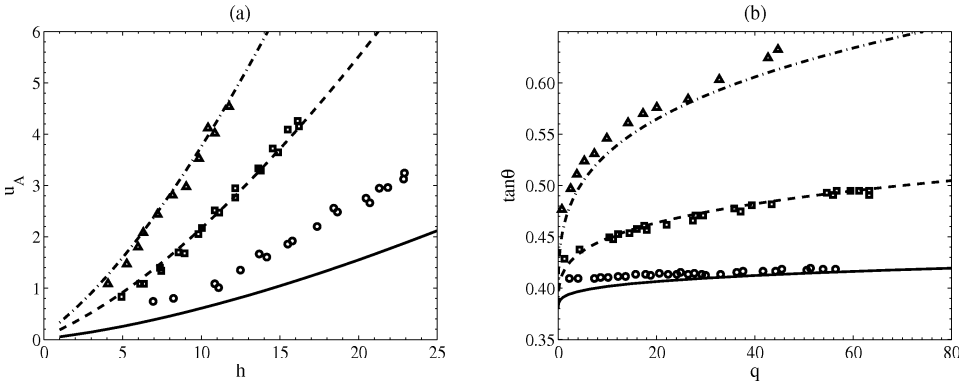

(a) (b)

FIGURE 3. (a) Theoretical (lines) and experimental (symbols) particle average velocity versus depth for dry granular flow ($Q = 0$) of glass spheres over a rigid, bumpy bed, without sidewalls, when $\theta = 22°$ (solid line and circles), $\theta = 25°$ (dashed line and squares), $\theta = 28°$ (dot-dashed line and triangles). (b) Theoretical (lines) and experimental (symbols) angle of inclination of the free surface versus particle volume flux for dry granular flow ($Q = 0$) of glass spheres over an erodible bed between frictional sidewalls when $W = 283$ (solid line and circles), $W = 57$ (dashed line and squares), $W = 19$ (dot-dashed line and triangles).

sidewalls. In this case, (2.16) implies that μ is constant in the flow and equal to $\tan\theta$. Here, only the experimental results of Pouliquen (1999*b*) for angles of inclination of his rigid, bumpy bed equal to 22°, 25° and 28° are reported. The theory fits the experimental results very well, except for the mildest slope, where the latter are underestimated. This is probably due to the approximation that we make in the rheology for the value of the inertial parameter when $\mu = \check{\mu}$. As already stated, we take $I = 0$ there, while it should be greater than zero. This results in an underestimation of the shear rate and, therefore, of the velocity, when $\mu = \tan\theta$ is close to $\check{\mu}$ (for glass spheres, this is for values of θ close to 21°). Figure 3b shows the predictions of the theory against the experimental results for the dry granular flow of the same glass spheres used by Pouliquen (1999*b*) over the top of a heap when frictional sidewalls made of glass are present (Jop *et al.* 2005). Once again, the angle of inclination of the free surface versus the particle volume flux is well

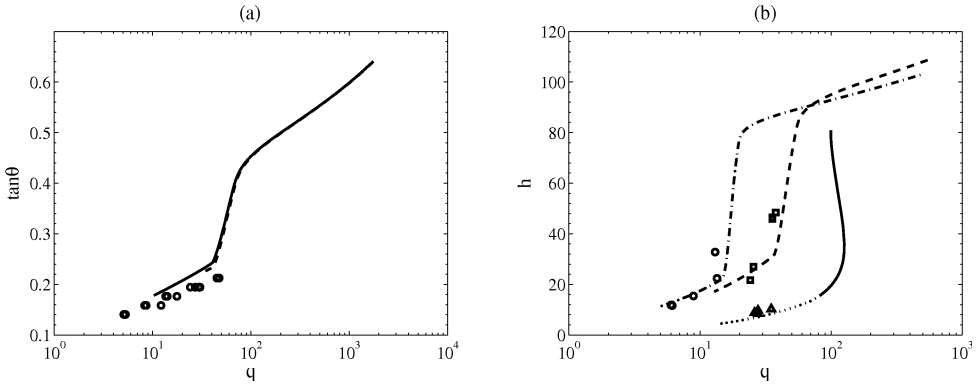

(a) (b)

FIGURE 4. (a) Experimental (circles) angle of inclination of the free surface versus particle volume flux for flows of glass spheres and water over an erodible bed between frictional sidewalls ($W = 67$) with $Q = 29$ and the theoretical predictions using the small-scale (dashed line) and the large-scale (solid line) turbulence. (b) Theoretical (lines) and experimental (symbols) particle depth versus particle volume flux for a flow of plastic cylinders and water between frictional sidewalls ($W = 54$) over an erodible bed with $Q = 8$ (dot-dashed line and circles), an erodible bed with $Q = 17$ (dashed line and squares), and a rigid bed of $\theta = 21^{\circ}$ with $Q = 32$ (solid line and triangles). The dotted line represents the results of the present theory for flows that can not be considered dense ($\mu_M > \hat{\mu}$).

predicted by the theory, for different values of the distance between the sidewalls.

In figure 4, we provide quantitative comparisons of the theory with experiments performed on steady, uniform flows of particles and water. Figure 4a shows the angle of inclination of the free surface as a function of the particle volume flux for a flow of glass spheres in water over an erodible bed. The experiments were performed by Tubino & Lanzoni (1993) in a channel of width $W = 67$ and sidewalls made of polycarbonate. The range of Q investigated in these experiments has been deduced from the experimental values of mean concentration $\bar{c}$ and particle flux through the relation $Q = q(1 - \bar{c})/\bar{c}$, suggested by the authors; this relation should hold approximately when h and H are close and the difference between the particle and the fluid velocity is small. The calculated

values of Q are in the range 16 to 41. The average value, $Q = 29$, has been employed to obtain the theoretical results of figure 4a. Analytical solutions for both the small- and large-scale turbulence approximation are shown in figure 4a. For the value of Q and for particles as heavy as glass spheres, the only appreciable effect of the turbulence expression is to change the minimum value of q for which the flow can still be considered to be dense (when the small-scale turbulence approximation is used, this minimum value of q is around 30; while, for the large-scale turbulence approximation, q can be as small as 10). It should be emphasized here that we have employed the same parameters in the particle rheology and the same wall friction coefficient obtained from the fitting with experiments performed on dry granular flows between glass sidewalls. No attempt has been made to modify these parameters to take into account the possible influence of the interstitial fluid or the fact that the sidewalls are made of polycarbonate instead of glass; we leave this to future work. Despite this, and the fact that the most of the experiments are in a range in which the flow cannot be considered dense, the agreement is quite good. In figure 4b, the comparisons between the experiments performed on flows of plastic cylinders and water over erodible and rigid beds by Armanini *et al.* (2005) and Larcher *et al.* (2007) are depicted together with the predictions of the present theory. The experimental data for the particle depth versus the particle volume flux have been obtained from the distributions of velocity and concentration obtained from optical measurements at the sidewall reported in Larcher *et al.* (2007). The value of Q has been obtained, as in the experiments of figure 4a, from the relation $Q = q(1 - \bar{c})/\bar{c}$. Five runs in the experimental campaign of Larcher *et al.* (2007) have been found to have a value of Q around 7, while, in the other five, Q ranges between 16 and 18. The values of Q used for obtaining the analytical solutions of figure 4b are, therefore, 7 and 17, respectively. The agreement with the experiments is notable, especially because the present theory

is capable of reproducing a key feature of steady, uniform granular–fluid flows that no existing single-phase theory can: the existence of a plateau for the particle volume flux, when the flow becomes under-saturated (see later in this section). In figure 4b, we show results of experiments performed by Armanini *et al.* (2005) over a rigid bed, with $\theta = 19$ to 23° and $Q = 25$ to 39 and compare this data with the predictions of the present theory for $\theta = 21^\circ$ and $Q = 32$. Unfortunately, the minimum value of q that corresponds to the maximum value of the stress ratio for which the flow can still be considered to be dense is around 70; while the experimental values are around 30. Nonetheless, if we use the present theory to solve the problem for such small values of q (dotted line of figure 4b), the agreement with the experiments is remarkable.

In the following, we show the predictions of the present theory for flows of water and the plastic cylinders used by Armanini *et al.* (2005) for values of the control parameters (q, Q, W, θ) not investigated by them. All the plots refer to solutions of the approximate theory for which the flow can be considered dense; so that the maximum value μ_M of the stress ratio in the flow is between $\check{\mu}$ and $\hat{\mu}$.

In figure 5, we provide graphs of the tangent of the angle of inclination of the free surface and the particle depth versus the particle volume flux for a channel width of 100 diameters for zero fluid volume flux - that is, a dry granular flow. In figure 5a, we show the angle of inclination versus the particle volume flux for the flow over an erodible bed, together with the curve for the flow over a rigid bed at an angle of inclination of 25°. The value of the particle volume flux at the intersection between the two curves separates the space of the particle volume fluxes in two regions. When the particle flux q is less than this value, both a flow over a rigid, bumpy bed and a flow over an erodible bed are possible at the same volume flux. In this case, as shown in figure 5b, the inclination of the erodible bed is less and the thickness of the flow above it is greater than for the rigid

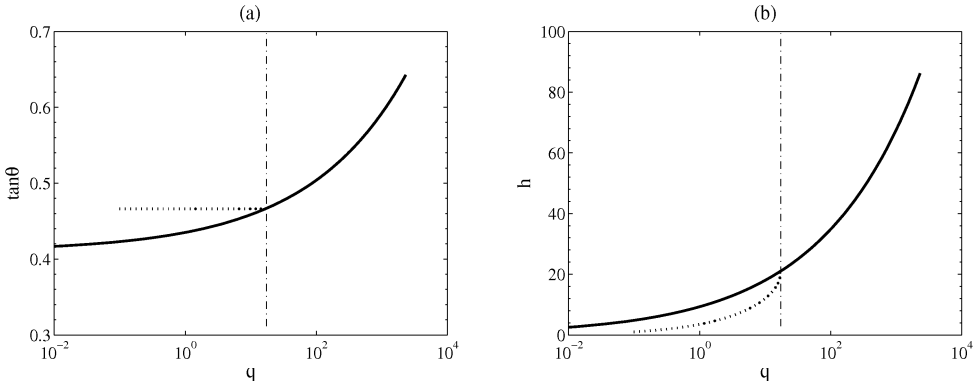

(a) (b)

FIGURE 5. (a) Particle volume flux versus angle of inclination in a channel of width $W = 100$ for a dry granular flow ($Q = 0$) over an erodible bed (solid line) and, with $\theta = 25^\circ$, over a rigid, bumpy bed (dotted line). (b) Particle volume flux versus depth in a channel of width $W = 100$ for a dry granular flow ($Q = 0$) over an erodible bed (solid line) and over a rigid, bumpy bed with $\theta = 25^\circ$ (dotted line).

bed. On the other hand, if we increase the particle volume flux beyond the value at the intersection, flow over a rigid bed becomes impossible; the flow develops an erodible bed at an angle of inclination greater than that of the rigid bed. This is the flow configuration that has been experimentally observed and modelled by Taberlet *et al.* (2003) and Jop *et al.* (2005). Finally, we note that the particle flux over an erodible bed tends to zero as $\tan\theta$ tends to $\breve{\mu}$ (in this case, 0.41). In other words, in the context of the model, flow over an erodible or a rigid bed is not possible if the angle of inclination of the bed is less than $\breve{\mu}$.

In figure 6, we show the more complicated results of adding a fluid volume flux, $Q = 50$, to the situations depicted in figure 5. There is still a limiting value of particle volume flux below which both a flow over a rigid bed and of a flow over an erodible bed, with the inclination of the latter less than that of the former, are possible. This situation has been experimentally observed by Armanini *et al.* (2005) and Fraccarollo, Larcher & Armanini

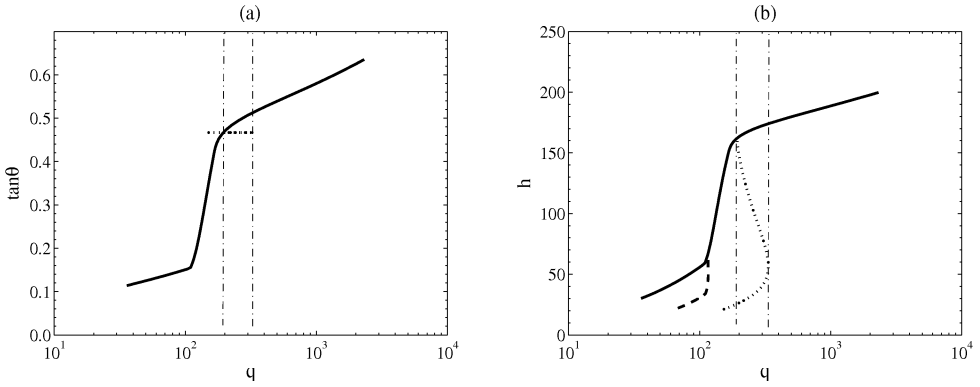

(a) (b)

FIGURE 6. (a) Same as in figure 5a, but $Q = 50$. (b) Same as in figure 5b, but $Q = 50$ and the flow over a rigid, bumpy bed is also shown for $\theta = 10^{\circ}$ (dashed line).

(2007). Also, there is still a limiting value of the particle flux beyond which only flow over an erodible bed is possible. Between these two limiting values, the theory predicts a range of particle volume fluxes for which three solutions are possible: two flows over a rigid bed and one over an erodible bed, with the inclination of the latter greater than those of the former (figure 6b). In absence of experimental evidence, we consider this as an artefact of our simplified treatment of the rigid boundary.

Figure 6a also shows that the curve for the flow over an erodible bed is S-shaped, with a nearly vertical plateau for a range of inclination angles (in this case, $0.2 < \tan\theta < 0.4$). In this range, q is nearly constant and, given that Q is fixed, the ratio $q/(q+Q)$ is also constant. This feature has been observed in the experiments of Armanini *et al.* (2005). Finally, in contrast with what we have observed for the dry granular flow, the particle flux in figure 6a does not tend asymptotically to a minimum as the angle of inclination is decreased. Indeed, by continuously decreasing the particle volume flux, keeping the fluid volume flux constant, we would approach the special case of a flow of a Newtonian fluid over an inclined surface. This flow can be steady and fully developed as long as the inclination of the free surface is not zero. Flows over a rigid bed with inclinations as small

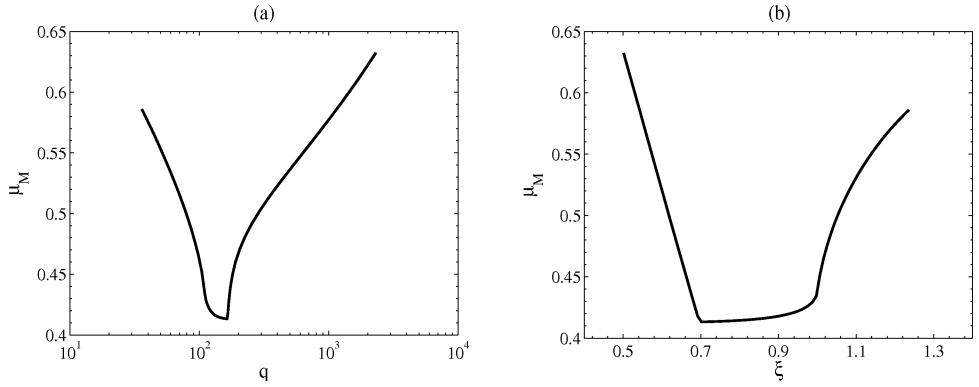

(a) (b)

FIGURE 7. (a) Maximum value of the stress ratio in the flow versus particle volume flux in a channel of width $W = 100$ for a granular–fluid flow ($Q = 50$) over an erodible bed. (b) Same as in figure 7a, but maximum stress ratio versus degree of saturation.

as 10°, i.e., for $\tan\theta$ much less than $\check{\mu}$, are, therefore, possible (figure 6b). In figure 7 we plot the predicted value of the maximum stress ratio in the flow against the particle volume flux and the degree of saturation for the granular–fluid flow over an erodible bed of figure 6. For a flow with a given Q to be considered dense ($\mu_M \leqslant \hat{\mu}$), q cannot exceed a maximum that corresponds to the minimum of the degree of saturation and cannot be less than a minimum that corresponds to the maximum in the degree of saturation.

An interesting feature of dry granular flows over an erodible bed between flat sidewalls has been highlighted by Jop *et al.* (2005). When the particle volume flux per unit width is scaled with the 5/2 power of the channel width, the experimental data of volume flux versus angle of inclination collapse onto a single curve. The theory outlined here is in agreement with this experimental observation. Indeed, if we substitute (2.17) in (2.19), with $u_p = 0$, we obtain the following universal relation for dry granular flows:

$$\frac{q}{W^{5/2}} = \frac{4\hat{c}}{35\chi\mu_w^{5/2}} (\cos\theta)^{1/2} (\tan\theta - \check{\mu})^{7/2} . \tag{3.1}$$

In order to see whether this scaling applies also to granular–fluid mixtures, we set the value of $Q/W^{5/2} = 5 \times 10^{-4}$ and, in figure 8a, plot the relation between $\tan\theta$ and $q/W^{5/2}$

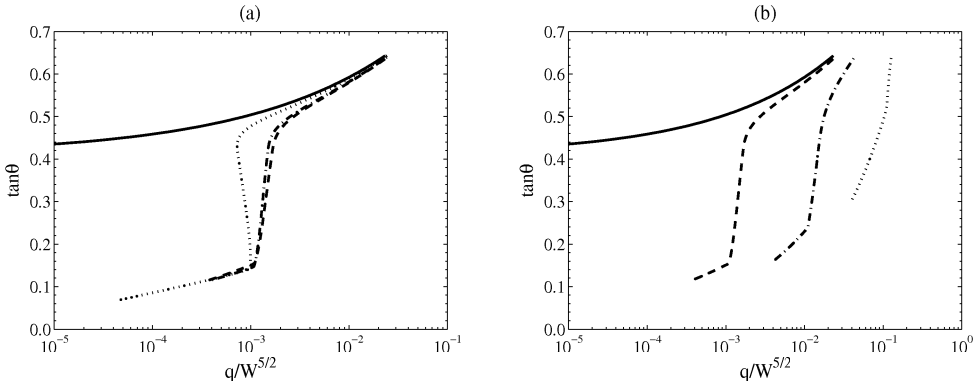

(a) (b)

FIGURE 8. (a) Scaled particle volume flux over an erodible bed versus angle of inclination for $W = 20$ (dotted line), $W = 50$ (dot-dashed line) and $W = 100$ (dashed line), with $Q/W^{5/2} = 5 \times 10^{-4}$. (b) Scaled particle volume flux over an erodible bed versus angle of inclination for $W = 100$, with $Q/W^{5/2} = 5 \times 10^{-4}$ (dashed line), $Q/W^{5/2} = 5 \times 10^{-3}$ (dot–dashed line) and $Q/W^{5/2} = 5 \times 10^{-2}$ (dotted line). In both figures, the solid line represents the universal relation (3.1) for dry granular flows.

obtained from the analytical expressions for flow over an erodible bed for channel widths of 20, 50 and 100 diameters, respectively. In the same figure, the relation (3.1) for dry granular flows is also shown. The scaling found by Jop *et al.* (2005) seems to apply to the granular–fluid mixture in the wider channels. When $W = 20$, the scaling breaks down in the plateau region. Instead of a plateau, there is a range of inclination angles for which multiple solutions to the flow over an erodible bed are possible. These involve three values of $\tan\theta$ for a given particle volume flux. It would be interesting to see whether such solutions are stable and whether they can be experimentally observed.

Figure 8a also shows that, as expected, when the particle volume flux is much greater than the fluid volume flux, the relation between particle volume flux and angle of inclination collapses onto the dry granular flow curve.

As shown in figure 8b, the transition to the dry granular flow curve takes place at higher values of $\tan\theta$ as the scaled fluid volume flux is increased. Moreover, the plateau tends to

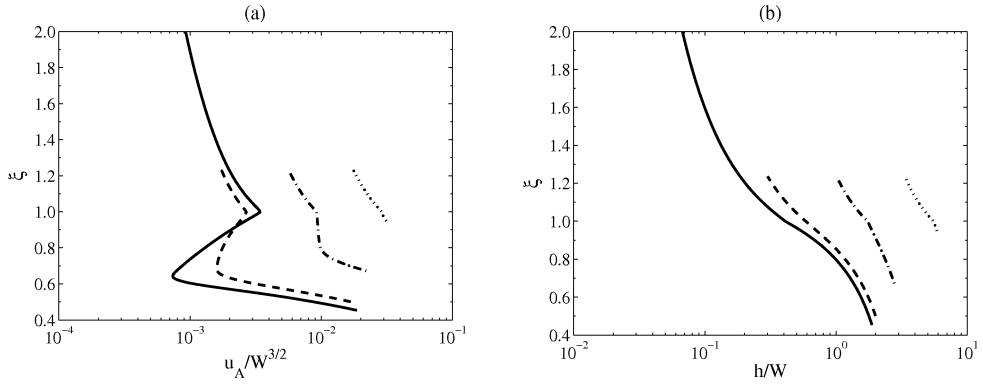

(a) (b)

FIGURE 9. (a) Scaled particle average velocity against degree of saturation in a flow over an erodible bed for $W = 20$ and $Q/W^{5/2} = 5 \times 10^{-4}$ (solid line), $W = 100$ and $Q/W^{5/2} = 5 \times 10^{-4}$ (dashed line), $W = 100$ and $Q/W^{5/2} = 5 \times 10^{-3}$ (dot-dashed line), and for $W = 100$ and $Q/W^{5/2} = 5 \times 10^{-2}$ (dotted line). (b) Same as in figure 9a, but scaled particle depth versus degree of saturation.

vanish with increasing fluid volume flux. To explain this behaviour, we plot, in figure 9a, the scaled particle average velocity $u_A/W^{3/2}$ against the degree of saturation ξ and, in figure 9b, the scaled depth h/W against ξ, for the three different fluid volume fluxes of figure 8b. Except for the case $Q/W^{5/2} = 5 \times 10^{-2}$, there is a range of under-saturated flows ($\xi \leqslant 1$) where $u_A/W^{3/2}$ is either constant or decreasing as ξ decreases, while h/W is always increasing as ξ decreases.

If saturated flows ($\xi = 1$) are possible for $\tan\theta < \breve{\mu}$, then there is a range of angle of inclination for which $\xi < 1$, the depth ψ of the dry shear layer is zero, and the plug extends between 0 and ζ. In this range, for channels that are not narrow, the decrease in the mean velocity, if present, is compensated for by the increase in the particle depth, and the particle volume flux is approximately constant. If, instead, the channel is narrow, the decrease in mean velocity is more important than the increase in particle depth, and the particle volume flux decreases as $\tan\theta$ increases (figure 8a). When $\tan\theta > \breve{\mu}$, as we

have shown in the previous section, the upper part of the surface dry granular layer of thickness ψ is sheared. This additional contribution to the mean velocity $u_A/W^{3/2}$ causes an increasing of the particle volume flux as $\tan\theta$ increases. If the condition $\xi = 1$ applies for $\tan\theta > \tilde{\mu}$, as for $Q/W^{5/2} = 5 \times 10^{-2}$, the entire upper dry layer is sheared, no plug develops in the flow, and the plateau vanishes.

3.2. *Steady, non-uniform, flow*

Here, we present the results for the steady, non-uniform flow of a mixture of water and the plastic cylinders used by Armanini *et al.* (2005) and described in the previous subsection. This allows us to employ the same values for the particle properties. Although such particles have not been used to perform experiments in steady, non-uniform condition, quite similar particles (PVC cylinders of specific weight $\sigma = 1.4$ and equivalent spherical diameter $d = 0.0046$ m) have been employed, as already mentioned, with water as interstitial fluid, by Davies (1988) in a moving-bed apparatus. Consequently, we expect that the theory will be able to provide predictions in, at least, qualitative agreement with the experiments.

The moving-bed apparatus of Davies (1988) was a rectangular flume 50 mm in width and 2 m in length, with its ends closed to retain both the fluid and the granular material. The channel bed was a corrugated nylon belt, driven by a system of rollers, and moving at a controlled, constant velocity. In the experiments, the belt velocity, the inclination of the channel, and the volumes of fluid and particles retained in granular–fluid mixture were the control parameters. As explained by Davies (1988), fixing the belt velocity in the apparatus was equivalent to fixing the average velocities $u_A = U_A$ of the flow in the laboratory frame of reference (figure 2). Setting the origin of the x-axis in figure 2 at the upward end of the flume and using the fluid and particle volumes V and v of (2.51) and (2.52) as control parameters allows us to mathematically mimic the experimental

apparatus of Davies (1988). In the apparatus, the mean velocity of the fluid and particles with respect to the sidewalls was zero. As suggested by Davies (1988), this implies that the frictional force exerted by the sidewalls on the particles was, on average, small. So, in this type of experimental set-up, it is not possible to investigate the influence of the channel width, W, on the flow. Consequently, the following predictions were obtained for $W = \infty$.

We employ a fourth-order Runge–Kutta method to solve the three differential equations (2.47), (2.48) and (2.49). In doing this, we adopt values of the control parameters, in particular, the average velocity and bed inclination, close to those employed by Davies (1988), but large enough to have a particle depth greater than 10 diameters for the most of the flow (see the second paragraph of the previous sub-section).

At each step in the Runga–Kutta method, we must evaluate the equilibrium angles Θ and θ for the fluid and the particles. To do this for known values of h and H at a given x, we evaluate ξ and, using the same iterative method employed for the steady, uniform flow introduced in the previous sub-section, we find the slope, corresponding to Θ or θ, that satisfies the condition on the average velocity for the fluid or the particles, respectively. The relative position of the fluid and particle snouts ($x^* - X^*$) and the origin of the x-axis in figure 2 depend on the values of the fluid and particle volumes, V and v. We tentatively set the relative position, $x^* - X^*$, of the snouts and integrate (2.45) and (2.46) upwards, starting from $x = x^*$ (or X^*, if it is downstream from x^*). At each step, we evaluate the particle volume per unit width and stop when it is sufficiently close to v. Then, we evaluate the fluid volume per unit width and, if not sufficiently close to V, we perform the integration again with a different value of $x^* - X^*$.

Figure 10 shows the influence of the particle and fluid volumes on the wave. In figure 10a, we plot the particle and fluid depth as a function of position x for different

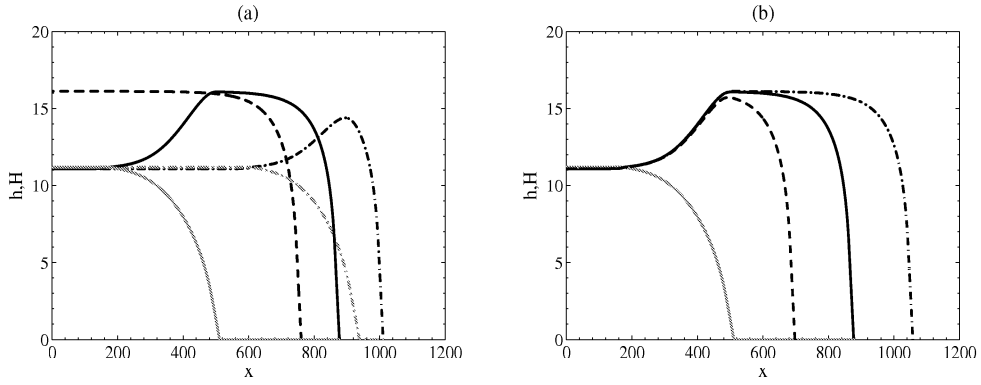

(a) (b)

FIGURE 10. (a) Particle depth (black lines) and fluid depth (gray lines) versus position for a granular–fluid wave over a rigid, bumpy bed with $\phi = 30°$, $u_A = U_A = 10$, $v = 8000$, and $W = \infty$, for $V = 0$ (dashed lines), $V = 1500$ (solid lines), and $V = 3000$ (dot-dashed lines). (b) Particle depth versus position for a granular–fluid wave over a rigid, bumpy bed with $\phi = 30°$, $u_A = U_A = 10$, $V = 1500$, and $W = \infty$, for $v = 6000$ (dashed line), $v = 8000$ (solid line), and $v = 10000$ (dot-dashed line). The fluid depth versus position, independent of the total particle volume v, is represented by the gray solid line.

values of V, while keeping $v = 8000$, with $\phi = 30°$ and $u_A = U_A = 10$. For $V = 0$, we have the results for a dry granular steady wave. The behaviour is similar to that obtained by Pouliquen (1999*a*) experimentally for $W = \infty$ and modelled by him using a different particle rheology from that employed here. The particle depth is zero at the wave front, then monotonically increases upwards, and tends, asymptotically, to a value $\hat{h}$ that is the depth of the steady, uniform, dry flow. When fluid is present ($V = 1500$), the solution shows some distinctive features of debris flows observed both in the laboratory (Davies 1988) and in nature (Takahashi 1991; Iverson 1997): (i) there is a part of the wave close to the snout in which the flow is dry; (ii) the wave exhibits a bulge at the front, with a maximum depth at about $x = X^*$; and (iii) moving upslope, both h and H tend to asymptotic values h_0 and H_0 which are the solutions for the steady, uniform flow. Figure 10a clearly shows that the bulging of the wave is a consequence of $\hat{h}$, to

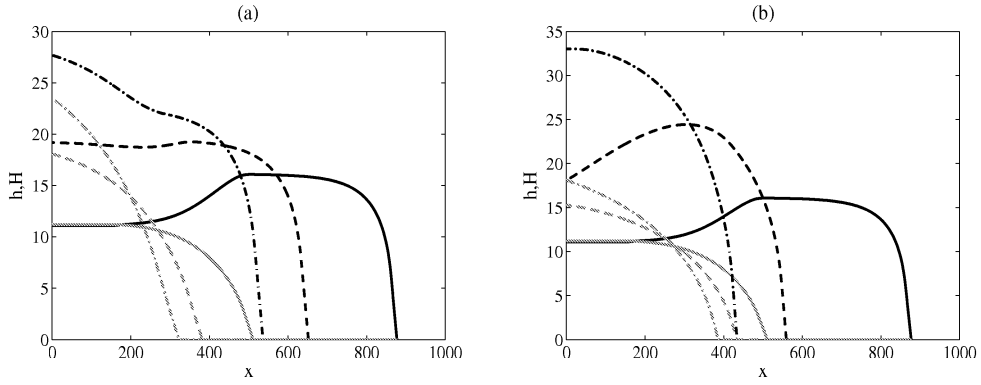

(a) (b)

FIGURE 11. (a) Particle depth (black lines) and fluid depth (gray lines) versus position for a granular–fluid wave over a rigid, bumpy bed with $\phi = 30°$, $v = 8000$, $V = 1500$, and $W = \infty$, for $u_A = U_A = 10$ (solid lines), $u_A = U_A = 13$ (dashed lines) and $u_A = U_A = 16$ (dot-dashed lines). (b) Particle depth (black lines) and fluid depth (gray lines) versus position for a granular–fluid wave over a rigid, bumpy bed with $u_A = U_A = 10$, $v = 8000$, $V = 1500$, and $W = \infty$, for $\phi = 20°$ (dot-dashed lines), $\phi = 25°$ (dashed lines) and $\phi = 30°$ (solid lines).

which the dry granular front tends, being, in this case, greater than h_0. If more fluid is added ($V = 3000$), both $x^* - X^*$ and the maximum depth of the bulge decrease.

In figure 10b, we plot the particle and fluid depth as a function of position x for different values of v, while keeping V constant, with $\phi = 30°$ and $u_A = U_A = 10$. The shapes are consistent with the observation made by Davies (1988) that the wave presents a front (head) in which the particle depth is increasing upslope, a body characterized by a constant depth, and a tail where the depth diminishes. Increasing the particle volume causes the length of the body to increase, without substantially affecting the shape of the front or the tail.

Finally, figure 11 shows the influence of the average velocity and bed inclination on the wave. Increasing the average velocity $u_A = U_A$ causes an increase in h_0 relative to $\hat{h}$ (figure 11a). Therefore, for a certain value of u_A, in this case 13, $h_0 \approx \hat{h}$, and the bulge disappears. For u_A greater than this value, $h_0 > \hat{h}$, and the granular–fluid wave depth is

monotonically increasing upslope, tending to an asymptotic value, as in the case of the uniformly progressive wave of a single-phase fluid (Hungr 2000). The fact that a bulbous granular–fluid wave is not always present was actually noticed by Davies (1988); here, we provide a rational explanation for this in the context of a simple, approximate theory. Figure 11b shows the effect of the bed inclination: the maximum depth of the wave increases if the bed inclination decreases, while $x^* - X^*$ diminishes (as already stated, no dry granular front is possible, if $\tan\phi < \breve{\mu}$).

4. Concluding remarks

In the present work, we completed the approximate analytical solutions (Berzi & Jenkins 2008*a*,*b*) for steady, uniform flows of gravity-driven granular–fluid mixtures, with or without frictional sidewalls, by extending them to situations in which the angle of inclination of the free surface is greater than the angle of repose of the solid material and to flows over a rigid bumpy bed. We then employed the analytical relations between particle and fluid average velocities, particle and fluid depths, and angle of inclination of the free surface to solve for the steady motion of a long granular–fluid wave over a rigid bumpy bed. Using a linear rheology with parameters that were previously evaluated through fitting with experiments (Berzi & Jenkins 2008*a*,*b*), we compared the predictions of the theory with existing experiments for steady, flows of water and plastic cylinders. We also made comparisons with experiments performed on steady, flows of glass spheres, with and without water, in many flow configurations.

Our theory reproduces many distinctive features of steady, uniform flows: (i) when frictional sidewalls are present, beyond a certain particle volume flux, the granular–fluid flow always develops an erodible bed at an angle of inclination greater than the rigid bed below, a phenomenon that has been observed by Taberlet *et al.* (2003); (ii) below this

particular value of particle volume flux, it is possible for the mixture to flow either over a rigid or an erodible bed, with the inclination of the latter less than that of the former, as experimentally observed by Armanini *et al.* (2005); and (iii) if the fluid volume flux is not too high, an under-saturated granular–fluid mixture flowing over an erodible bed is characterized by an almost constant ratio between particle volume flux and total volume flux over a wide range of angles of inclination, as noted by Armanini *et al.* (2005).

The theory also allowed us to qualitatively reproduce the experimental results on steady, non-uniform granular–fluid flows over a rigid bumpy bed performed by Davies (1988), using a moving-bed apparatus. For a certain range of angles of inclination of the rigid bed and average velocities of both fluid and particles, if the amount of particles is sufficiently large in comparison with that of fluid, then (i) the wave has a bulbous shape, with a dry granular front, a body of constant depth, and a tail which is slightly under-saturated; (ii) an increase in the amount of particles causes the length of the body to increase without substantially affecting either the front or the tail; and (iii) increases in the average velocity of fluid and particles eventually lead to the vanishing of the bulge, so that the granular–fluid wave depth is monotonically increasing upslope, as is the case for a single-phase fluid.

The approximate theory is based on the fundamental assumption that the depth of the dense flow is sufficiently large (e.g.at least 10 diameters thick) to disregard the influence of boundaries on the energy balance of the particles. This leads to algebraic relations between the particle stress ratio, inertial parameter, and concentration; that is, a 'local rheology' for the particles. Also, for the local rheology to be approximately linear, most of the flow must be dense. Despite these drawbacks, the relative simplicity of the theory and the good qualitative and quantitative agreement of its predictions with experiments

on steady flows, even well beyond its expected range of applicability, seem promising with respect to its practical applications in the field of civil engineering.

We are grateful to Professor E. Larcan for his continued interest in this work. J. T. Jenkins acknowledges financial support from the Region of Lombardia and the hospitality of the Section of Hydraulics of the D.I.I.A.R. Department at the Politecnico di Milano.

Appendix A

In order to derive the analytical solution for a steady, uniform flow of a gravity-driven granular–fluid mixture when no sidewalls are present, we use the assumptions of constant concentration ($c = \hat{c}$) and similarity of the velocity profiles ($u' = U'$). First, we employ the drag force (2.7) in the particle flow momentum balance (2.9), in which we set $\mu_w = 0$. Upon integrating, we obtain the distribution of the particle shear stress:

$$s = s^* + [\hat{c} + (1 - \hat{c})/\sigma]\,[z - h\,(1 - \alpha)]\sin\theta - S + S^*, \tag{A 1}$$

where s^* and S^* are, respectively, the particle and fluid shear stresses at $z = h(1 - \alpha)$:

$$s^* = h(1 - \alpha)\hat{c}\sin\theta \tag{A 2}$$

and

$$S^* = h(\beta - 1)\sin\theta/\sigma. \tag{A 3}$$

Similarly, we integrate (2.8) to obtain the distribution of the particle pressure:

$$p = \{z - [z - h(1 - \alpha)]\,/\sigma\}\,\hat{c}\cos\theta. \tag{A 4}$$

With the approximation (2.10) or (2.11) for the fluid shear stress, the ratio of particle shear stress and pressure is, from (A 1) and (A 4) and the condition $u' = U'$,

$$\mu = \frac{z + (1 - \hat{c})\,[z - h(1 - \alpha)]\,/(\hat{c}\sigma)}{z - [z - h(1 - \alpha)]\,/\sigma}\tan\theta - D^2 I^2$$

$$+\frac{S^*}{\{z-[z-h(1-\alpha)]/\sigma\}\,\hat{c}\cos\theta}. \tag{A 5}$$

With the linear rheology (2.1), we rewrite (A 5) as

$$DI^2+\chi I+\frac{\chi^2}{4D}-\frac{2Fz+N}{z+L}=0. \tag{A 6}$$

Upon taking $I=0$ in (A 6), we may determine the value $z=\zeta$ (the base of the plug) for which $\mu=\breve{\mu}$ reported in table 2.

The quadratic (A 6) may be solved for I and integrated with the boundary condition $u(h)=u_b$ to obtain the particle velocity profile:

$$\begin{aligned} u=u_b&-\chi[(1-1/\sigma)\cos\theta]^{1/2}\left[(h+L)^{3/2}-(z+L)^{3/2}\right]/(3D)\\ &-[(1-1/\sigma)\cos\theta]^{1/2}\left[(2Fz+N)^{3/2}-(2Fh+N)^{3/2}\right]/\left(3FD^{1/2}\right). \end{aligned} \tag{A 7}$$

Integrating again between ζ and h, we obtain the mean value u_m of the particle velocity in the flow layer reported in table 2. In the upper plug layer, $\psi\leqslant z\leqslant\zeta$, the particle velocity u_p is constant and equal, for continuity, to $u(\zeta)$. Given that μ_w is zero, the upper dry layer in an under-saturated flow is either totally sheared if $\tan\theta>\breve{\mu}$ or not sheared at all if $\tan\theta\leqslant\breve{\mu}$, so that ψ has the expression reported in table 2.

Finally, the distribution of μ with z and, consequently, also its value μ_b at $z=h$, reported in table 2, can be obtained by substituting the linear rheology (2.1) in (A 6).

Appendix B

Here we provide only the derivation of the average inertial term for the fluid. The derivation for the average inertial term for the particles is straightforward.

We first use the Leibniz's rule, to obtain

$$\begin{aligned} \frac{1}{\sigma}\int_h^{\beta h}\frac{\mathrm{d}U}{\mathrm{d}t}\mathrm{d}Z+\frac{1-\hat{c}}{\sigma}\int_0^{\alpha h}\frac{\mathrm{d}U}{\mathrm{d}t}\mathrm{d}Z&=\frac{1}{\sigma}\frac{\partial}{\partial t}\left[\int_h^{\beta h}U\mathrm{d}Z+(1-\hat{c})\int_0^{\alpha h}U\mathrm{d}Z\right]\\ &+\frac{1}{\sigma}\frac{\partial}{\partial x}\left[\int_h^{\beta h}U^2\mathrm{d}Z+(1-\hat{c})\int_0^{\alpha h}U^2\mathrm{d}Z\right] \end{aligned}$$

$$-\frac{1}{\sigma}U(\beta h)\left[\frac{\partial(\beta h)}{\partial t}+U(\beta h)\frac{\partial(\beta h)}{\partial x}-U_z(\beta h)\right]$$
$$-\frac{1-\hat{c}}{\sigma}U(\alpha h)\left[\frac{\partial(\alpha h)}{\partial t}+U(\alpha h)\frac{\partial(\alpha h)}{\partial x}-U_z(\alpha h)\right]$$
$$+\frac{1}{\sigma}U(h)\left[\frac{\partial h}{\partial t}+U(h^+)\frac{\partial h}{\partial x}-U_z(h^+)\right], \qquad (B\,1)$$

where U_z is the fluid velocity in the Z-direction and the index $+$ indicates that the quantity is evaluated by approaching $Z = h$ from above. In (B 1) we have made use of the incompressibility of the fluid and the rigidity of the bottom ($Z = 0$) boundary.

For over-saturated flows ($\alpha = 1$), $Z = \beta h$ is a material boundary for the fluid; hence $\partial(\beta h)/\partial t + U(\beta h)\partial(\beta h)/\partial x - U_z(\beta h) = 0$, $U(\alpha h) = U(h^-)$ and $U_z(\alpha h) = U_z(h^-)$. If we apply the fluid mass balance to a pillbox on the interface at $Z = h$, we obtain the jump condition:

$$\frac{\partial h}{\partial t}+U(h^+)\frac{\partial h}{\partial x}-U_z(h^+)-(1-\hat{c})\left[\frac{\partial h}{\partial t}+U(h^-)\frac{\partial h}{\partial x}-U_z(h^-)\right]. \qquad (B\,2)$$

Therefore, the last three terms in (B 1) vanish. The same holds for under-saturated flows ($\beta = 1$), because, in this case, $U(\beta h) = U(h^+)$, $U_z(\beta h) = U_z(h^+)$, and $Z = \alpha h$ is a material boundary for the fluid; hence $\partial(\alpha h)/\partial t + U(\alpha h)\partial(\alpha h)/\partial x - U_z(\alpha h) = 0$. Using the definition of average velocity U_A given in (2.25), we may write (B 1) as:

$$\frac{1}{\sigma}\int_h^{\beta h}\frac{\mathrm{d}U}{\mathrm{d}t}\mathrm{d}Z+\frac{1-\hat{c}}{\sigma}\int_0^{\alpha h}\frac{\mathrm{d}U}{\mathrm{d}t}\mathrm{d}Z=\frac{1}{\sigma}\frac{\partial}{\partial t}\left\{U_A h\left[\beta-1+\alpha(1-\hat{c})\right]\right\}$$
$$+\frac{1}{\sigma}\frac{\partial}{\partial x}\left\{U_A^2 h\left[\beta-1+\alpha(1-\hat{c})\right]\right\}. \qquad (B\,3)$$

This holds only approximately, because we have assumed the trivial correlation:

$$\frac{\int_h^{\beta h}U^2\mathrm{d}Z+(1-\hat{c})\int_0^{\alpha h}U^2\mathrm{d}Z}{U_A^2 h\left[\beta-1+\alpha(1-\hat{c})\right]}=1. \qquad (B\,4)$$

Actually, this ratio is in the range 1 to 1.5 for a steady, uniform flow (using the analytical solution provided in table 1 or 2), so we do not expect this approximation has a great influence on the solution for a steady, non-uniform flow. Finally, using the fluid mass

balance,

$$\frac{\partial\left\{h\left[\beta-1+\alpha(1-\hat{c})\right]\right\}}{\partial t}+\frac{\partial\left\{U_A h\left[\beta-1+\alpha(1-\hat{c})\right]\right\}}{\partial x}=0, \tag{B 5}$$

in (B 3), we obtain (2.32).

REFERENCES

Ancey, C. 2007 Plasticity and geophysical flows: A review. *J. Non-Newton. Fluid* **14**, 4–35.

Armanini, A., Capart, H., Fraccarollo, L. & Larcher, M. 2005 Rheological stratification in experimental free-surface flows of granular-liquid mixtures. *J. Fluid Mech.* **532**, 269–319.

Bagnold, R.A. 1954 Experiments on a gravity-free dispersion of large solid spheres in a newtonian fluid under shear. *Proc. R. Soc. London A* **225**, 49–63.

Berzi, D. & Jenkins, J.T. 2008*a* Approximate analytical solutions in a model for highly concentrated granular–liquid flows. *Phys. Rev. E* **78**, 011304.

Berzi, D. & Jenkins, J.T. 2008*b* A theoretical analysis of free-surface flows of saturated granular–liquid mixtures. *J. Fluid Mech.* **608**, 393–410.

Cassar, C., Nicolas, M. & Pouliquen, O. 2005 Submarine granular flows down inclined planes. *Phys. Fluids* **17**, 103301.

Chen, C.L. & Ling, C.H. 1998 Rheological equations in asymptotic regimes of granular flow. *J. Engrg. Mech.* **124** (3), 301–310.

Chow, V.T. 1959 *Open channel hydraulics*. McGraw-Hill.

da Cruz, F., Sacha, E., Prochnow, M., Roux, J. & Chevoir, F. 2005 Rheophysics of dense granular materials : Discrete simulation of plane shear flows. *Phys. Rev. E* **72**, 021309.

Dallavalle, J. 1943 *Micromeritics*. Pitman.

Davies, T.R.H. 1988 Debris Flow Surges A Laboratory Investigation. *Mitteilungen der Versuchsanstalt für Wasserbau, Hydrologie und Glaziologie* 96. Technischen Hochschule Zürich.

Davies, T.R.H. 1990 Debris flow surges-experimental simulation. *J Hydrol. (New Zealand)* **29**, 18–46.

Drew, D.A. & Passman, S.L. 1999 *Theory of Multicomponent Fluids*. Springer.

Fraccarollo, L., Larcher, M. & Armanini, A. 2007 Depth-averaged relations for granular-

liquid uniform flows over mobile bed in a wide range of slope values. *Granul. Matter* **9**, 145–157.

GDR MiDi 2004 On dense granular flows. *Eur. Phys. J. E* **14**, 341–365.

Goldhirsch, I. 2003 Rapid granular flows. *Annu. Rev. Fluid Mech.* **35**, 267–293.

Hungr, O. 2000 Analysis of debris flow surges using the theory of uniformly progressive flow. *Earth Surf. Process. Landf.* **25**, 483–495.

Hunt, B. 1984 Perturbation solution for dam-break floods. *J. Hydr. Engrg.* **110** (8), 1058–1071.

Hunt, B. 1994 Newtonian fluid mechanics treatment of debris flows and avalanches. *J. Hydr. Engrg.* **120** (12), 1350–1363.

Iverson, R. M. 1997 The physics of debris flows. *Rev. of Geophysics* **35** (3), 245–296.

Jenkins, J.T. 2001 Boundary conditions for collisional grain flows at bumpy, frictional boundaries. In *Granular gases* (ed. T. Poschel & S. Luding), pp. 125–139. Springer.

Jenkins, J.T. 2006 Dense shearing flows of inelastic disks. *Phys. Fluids* **18**, 103307.

Jenkins, J.T. 2007 Dense inclined flows of inelastic spheres. *Granul. Matter* **10**, 47–52.

Jenkins, J.T. & Askari, E. 1991 Boundary conditions for granular flows: phase interfaces. *J. Fluid Mech.* **223**, 497–508.

Jenkins, J.T. & Askari, E. 1999 Hydraulic theory for a debris flow supported on a collisional shear layer. *Chaos* **9**, 654.

Johnson, P.C. & Jackson, R. 1987 Frictional–collisional constitutive relations for granular materials, with application to plane shearing. *J. Fluid Mech.* **176**, 67–93.

Jop, P., Forterre, Y. & Pouliquen, O. 2005 Crucial role of sidewalls in granular surface flows: consequences for the rheology. *J. Fluid Mech.* **541**, 167–192.

Komatsu, T.S., Inagaki, S., Nakagawa, N. & Nasuno, S. 2001 Creep motion in a granular pile exhibiting steady surface flow. *Phys. Rev. Lett.* **86**, 1757–1760.

Larcher, M., Fraccarollo, L., Armanini, A. & Capart, H. 2007 Set of measurement data from flume experiments on steady, uniform debris flows. *J. Hydr. Res.* **45** (extra).

de Marsily, G. 1981 *Quantitative hydrogeology: groundwater hydrology for engineers*. Academic press.

Mitarai, N. & Nakanishi, H. 2005 Bagnold scaling, density plateau, and kinetic theory analysis of dense granular flow. *Phys. Rev. Lett.* **94**, 128001.

Mitarai, N. & Nakanishi, H. 2007 Velocity correlations in dense granular shear flows: Effects on energy dissipation and normal stress. *Phys. Rev. E* **75**, 031305.

Pouliquen, O. 1999*a* On the shape of granular fronts down rough inclined planes. *Phis. Fluids* **11** (7), 1956–1958.

Pouliquen, O. 1999*b* Scaling laws in granular flows down rough inclined planes. *Phis. Fluids* **11** (3), 542–548.

Richard, P., Valance, A., Mtayer, J.-F., Sanchez, P., Crassous, J., Louge, M. & Delannay, R. 2009 Rheology of confined granular flows: scale invariance, glass transition, and friction weakening. *Phys. Rev. Lett.* **101**, 248002.

Richardson, J. F. & Zaki, W. N. 1954 Sedimentation and fluidization, part 1. *Trans. Instn. Chem. Engrs.* **32**, 35–53.

Richman, M.W. 1988 Boundary conditions based on a modified maxwellian velocity distribution function for flows of identical, smooth, nearly elastic spheres. *Acta Mech.* **75**, 227.

Savage, S. B. & Hutter, K. 1989 The motion of a finite mass of granular material down a rough incline. *J. Fluid Mech.* **199**, 177–215.

Silbert, L. E., Ertas, D., Grest, G. S., Halsey, T. C., Levine, D. & Plimpton, S. J. 2001 Granular flow down an inclined plane: Bagnold scaling and rheology. *Phys. Rev. E* **64**, 51302.

Taberlet, N., Richard, P., Valance, A., Losert, W., Pasini, J.M., Jenkins, J.T. & Delannay, R. 2003 Superstable granular heap in a thin channel. *Phys. Rev. Lett.* **91**, 264301.

Takahashi, T. 1991 *Debris flow.* IAHR Monograph Series. Balkema.

Tubino, M. & Lanzoni, S. 1993 Rheology of debris flows: experimental observations and modelling problems. *Excerpta Ital. Contrib. Field Hydraul. Eng.* **7**, 201–236.